SECURITY INFORMATION
CONFIDENTIAL

289

Copy
RM L53B26

NACA RM L53B26

NACA

RESEARCH MEMORANDUM

LOW-SPEED AILERON EFFECTIVENESS AS DETERMINED BY FORCE TESTS AND VISUAL-FLOW OBSERVATIONS ON A 52° SWEPTBACK WING WITH AND WITHOUT CHORD-EXTENSIONS

By Patrick A. Cancro

Langley Aeronautical Laboratory
Langley Field, Va.

CLASSIFICATION CHANGED TO UNCLASSIFIED
AUTHORITY: NACA RESEARCH ABSTRACT NO. 97
DATE: FEBRUARY 24, 1956
WHL

CLASSIFIED DOCUMENT

This material contains information affecting the National Defense of the United States within the meaning of the espionage laws, Title 18, U.S.C., Secs. 793 and 794, the transmission or revelation of which in any manner to an unauthorized person is prohibited by law.

NATIONAL ADVISORY COMMITTEE
FOR AERONAUTICS

WASHINGTON
April 29, 1953

CONFIDENTIAL

NATIONAL ADVISORY COMMITTEE FOR AERONAUTICS

RESEARCH MEMORANDUM

LOW-SPEED AILERON EFFECTIVENESS AS DETERMINED BY FORCE TESTS AND VISUAL-FLOW OBSERVATIONS ON A 52° SWEPTBACK WING WITH AND WITHOUT CHORD-EXTENSIONS

By Patrick A. Cancro

SUMMARY

A low-speed investigation has been conducted in the 19-foot pressure tunnel at Reynolds numbers of 5.5×10^6 and 1.3×10^6 to determine the effect of leading-edge chord-extensions on the aileron characteristics of a 52° sweptback wing. The wing had an aspect ratio of 2.83, a taper ratio of 0.617, and symmetrical circular-arc airfoil sections, and was equipped with a 0.495-semispan aileron which extended from 0.415 to 0.910 semispan. In an attempt to simulate a more centrally located aileron, the outboard portion of the aileron was fixed to the wing and the resulting 0.370-semispan aileron was tested.

The results of the investigation indicate that the values of the aileron effectiveness parameter C_{l_δ} on the plain wing at zero lift for ailerons of 0.495 and 0.370 semispan were 0.00085 and 0.00063, respectively. However, at maximum lift the values of C_{l_δ} were approximately 65 percent of the values obtained at zero lift for each configuration. Although the leading-edge flow was markedly changed with the addition of chord-extensions, the lateral control characteristics, except for very high negative aileron deflections and low angles of attack, were not materially different from those obtained on the plain wing. This was true for the wing equipped with either the 0.495-semispan or the 0.370-semispan aileron.

INTRODUCTION

Outboard leading-edge chord-extensions have proved to be an effective means for improving the longitudinal stability characteristics

of sweptback wings which experience leading-edge separation (for example, see ref. 1). The manner in which the leading-edge flow on such wings (described in ref. 2) is altered by chord-extensions could be expected to produce significant changes in the flow over outboard ailerons. In contrast to the case of the wing without chord-extensions, where the low-energy boundary-layer air trails off at the wing tips, the addition of chord-extensions creates a vortex which causes the low-energy air from the inboard sections to trail off the wing at a spanwise station slightly outboard of the inboard end of the chord-extensions.

An investigation has been conducted in the Langley 19-foot pressure tunnel to show the effects of the flow changes produced by chord-extensions on the effectiveness of ailerons located outboard on a highly sweptback wing. In an attempt to give a better understanding of any changes in forces and moments produced by chord-extensions, visual observations of the boundary-layer flow on the wing were made by releasing a solution of lampblack and kerosene at various points on the upper surface of the wing.

This paper presents the aileron control characteristics obtained with and without leading-edge chord-extensions on a 52° sweptback wing of aspect ratio 2.83 with circular-arc airfoil sections. For comparative purposes, similar results obtained from tests of the wing equipped with extensible leading-edge flaps are also included.

The force and moment investigation was conducted at a Reynolds number of 5.5×10^6 and a Mach number of 0.11 for an angle-of-attack range from 0° through stall. The visual-flow investigation was conducted at a Reynolds number of 1.3×10^6 and a Mach number of 0.065 for an angle-of-attack range from 0° through stall.

SYMBOLS

C_L	lift coefficient, Lift/qS
C_m	pitching-moment coefficient about $0.25\bar{c}$, Pitching moment/$qS\bar{c}$
C_l	rolling-moment coefficient, Rolling moment/qSb
C_n	yawing-moment coefficient, Yawing moment/qSb
S	wing area, sq ft
$\bar{c}$	mean aerodynamic chord, $\frac{2}{S}\int_0^{b/2} c^2 dy$, ft

b	wing span, ft
c	local chord measured parallel to the plane of symmetry, ft
y	spanwise ordinate, ft
q	free-stream dynamic pressure, $\frac{1}{2}\rho V^2$, lb/sq ft
V	free-stream velocity, ft/sec
ρ	mass density of air, slugs/cu ft
R	Reynolds number
M	Mach number
α	angle of attack, deg
δ_a	aileron deflection measured in a plane perpendicular to the hinge line, deg
C_{l_δ}	variation of rolling moment with aileron deflection
Q	moment area, $S_a\bar{y}$
S_a	area of aileron
$\bar{y}$	distance from centroid of area to plane of symmetry

Subscripts:

0.495	for 0.495-semispan aileron
0.370	for 0.370-semispan aileron

MODEL

A plan view of the wing and some of the geometric characteristics are given in figure 1. The wing had an aspect ratio of 2.83, a taper ratio of 0.617, and an angle of sweepback of 52.05° along a straight line connecting the leading edges of the root chord and the theoretical tip chord. Each wing was fabricated from a solid steel blank by making both the upper and the lower surface a section of a cylinder with a radius of 83.26 inches. The leading and trailing edges of the wings are sections of an ellipse formed by the intersection of two cylinders,

the axes of which intersect at the proper angle to produce the desired taper ratio. The maximum thickness of the wing in a plane normal to the 0.50-chord line was 9.77 percent of the chord at the root and 6.11 percent of the chord at the tip. In a plane parallel to the plane of symmetry, the wing had a thickness of 6.52 percent at the root and 4.05 percent at the tip. The wing had no geometric twist or dihedral.

The left side of the wing was equipped with a flap-type aileron (fig. 2). The aileron chord was about 0.18c and the span was 0.495b/2. The outboard portion of the aileron could be fixed to the wing in such a manner as to permit a 0.370b/2-span aileron to be tested. The inboard end of the aileron was located at 0.415b/2, measured from the plane of symmetry. The aileron was sealed with cellophane tape for all tests except those made for the visual-flow studies.

Details of the leading-edge chord-extensions and extensible leading-edge flaps are shown in figure 2. Their spans extended inboard from the 0.975b/2 to the 0.725b/2 station. The chord-extensions were extended forward of the leading edge approximately 0.17c and faired into the airfoil sections. The extensible leading-edge flaps were of constant chord and had a 37° angle of incidence measured from the wing chord line in a plane perpendicular to a line joining the leading edges of the root and tip chords.

TESTS

The force tests were conducted in air compressed to an absolute pressure of 33 pounds per square inch at a Reynolds number of 5.5×10^6 and a Mach number of 0.11. Visual-flow studies were made in air at atmospheric pressure at a Reynolds number of 1.3×10^6 and a Mach number of 0.065. Some visual-flow tests were made at a value of Reynolds number of 3.0×10^6 to ascertain whether the flow patterns obtained at a Reynolds number of 1.3×10^6 could be considered representative of data obtained at much higher Reynolds numbers.

Lift and pitching, rolling, and yawing moments were obtained through an angle-of-attack range from 0° to an angle of attack beyond maximum lift for the plain wing and the wing equipped with leading-edge devices. The aileron deflection range was from -25° to 25°.

CORRECTIONS

All data have been reduced to standard nondimensional coefficients. Stream inclination and jet-boundary corrections have been applied to the

angle of attack. Jet-boundary corrections have been applied to the pitching-moment and rolling-moment data (ref. 3). The rolling-moment coefficient C_l varied with angle of attack α for each configuration with $\delta_a = 0^\circ$ (see fig. 3). The results for the various configurations are similar and indicate that the asymmetry due either to the wing or to the air stream was not constant throughout the angle-of-attack range. In an attempt to determine the cause of this variation, the wing was inverted and was tested through the angle-of-attack range. The data obtained were found to be essentially the same as those obtained with the wing erect. As a result, the variation of C_l with α is probably due to an asymmetry of the air stream which is not constant with angle of attack. In order to present data without the effects of tunnel air-stream asymmetry, values obtained from the faired curves shown in figure 3 were applied as tares.

RESULTS

Visual-flow studies on the plain wing and the wing equipped with leading-edge chord-extensions are shown photographically in figures 4 and 5. The lift and the rolling-, pitching-, and yawing-moment characteristics obtained for the plain wing configuration with a 0.370- and a 0.495-semispan aileron are presented in figures 6 and 7. Similar data are presented in figures 8 and 9 for the wing equipped with chord-extensions and in figures 10 and 11 for the wing with extensible leading-edge flaps. Representative cross plots of C_l against aileron deflection δ_a are presented in figures 12 and 13. The values obtained from the curves of C_l plotted against δ_a were used as the basis for the fairings of the curves of C_l plotted against α. Some scatter was encountered but it did not appear to affect materially the trends. In order to show the aileron effectiveness for a small range of aileron deflections through $\delta_a = 0^\circ$, variations of C_{l_δ} with angle of attack are presented in figure 14.

DISCUSSION

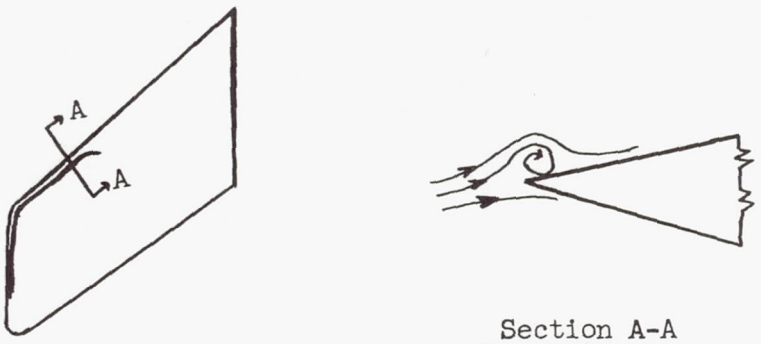
Visual-Flow Studies

An opaque liquid was used in the visual-flow studies in the boundary layer over the swept wing as presented in this paper. The investigation was made during the early stages of that testing technique in the Langley 19-foot pressure tunnel, and as such the results obtained are not as complete as presently possible. These studies were made at a

Reynolds number of 1.3×10^6 after tests at a Reynolds number of 3.0×10^6 had indicated no appreciable difference in flow patterns.

As pointed out in reference 2, the changes in section lift characteristics brought about by the leading-edge-vortex flow on swept wings with sharp leading edges produce changes in the pitching-moment characteristics throughout the angle-of-attack range. It was of interest in the present investigation to determine from visual-flow observations the location of the vortex and to define its path as it moved over the wing. The procedure employed was to allow a solution of lampblack and kerosene to flow into the boundary layer through a tube at the end of a strut-mounted probe. It was possible to move this probe spanwise and chordwise at will, as can be seen in figure 5. In this investigation, except for the condition shown in figure 5, the solution was released at a chordwise position of approximately 0.05c and a spanwise position of 0.50b/2 for the configurations with and without chord-extensions. In addition, the solution was released at the inboard leading edge of the chord-extension. The results obtained are shown photographically as figure 4. The interpretation of the flow studies is as follows:

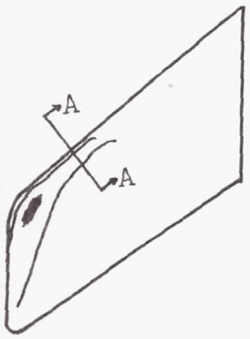
When the leading-edge separation vortex (such as described in ref. 2) enveloped the chordwise position at which the solution was released, the solution flowed outboard and forward until it reached the position where the vortex was lifting off the surface and then flowed outboard as shown in figure 4(d) and the following sketch:

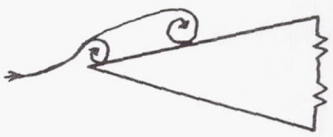


Section A-A

It may be noted that as the angle of attack was increased, the leading edge of the vortex moved chordwise away from the leading edge of the tip sections, leaving an area of diffused flow as shown by the darkened area at the leading edge of the tip sections (fig. 4(f)). Although it is not clearly illustrated, a rivulet of the solution was

observed flowing along the leading edge, which indicated the presence of a secondary vortex, as in the following sketch:





Section A-A

There is no evidence of a vortex on the basic wing at $\alpha = 0^\circ$ (see fig. 4(a)). In all probability a leading-edge vortex is present at $\alpha = 2^\circ$ as a result of the sharp leading edge, but as can be seen in figure 4(b), it had not developed enough to engulf the position at which the solution was released. The initial break in the pitching-moment curve occurs at approximately $\alpha = 4^\circ$, at which angle of attack the vortex has increased in size (fig. 4(c)). With an increase in angle of attack from 4° to 8°, the leading edge of the vortex is still moving along the leading edge of the wing. From reference 2, it was determined that the vortex is expanding chordwise, resulting in an increase in lift at the tip sections and a stabilizing effect on the wing. At $\alpha = 10^\circ$ the leading edge of the vortex has moved back from the leading edge of the tip sections and has proceeded to move inboard (fig. 4(f)). With further increase in angle of attack (figs. 4(h) to 4(l)), the vortex continues to move inboard and leaves the tips in a diffused region of flow, so that a decrease in lift results. Contrarily, the inboard sections of the wing, because the vortex is stronger, are experiencing an increase in lift that results in a destabilizing pitching moment throughout the moderate to high lift range.

With the addition of leading-edge chord-extensions to the wing, a stablizing effect on the pitching-moment characteristics is realized. (Compare figs. 6 and 8 and figs. 7 and 9.) In the case of the swept wing, especially with a sharp leading edge, separation occurs at very low lift coefficients. The action of the chord-extension vortex off the inboard end is such that the leading-edge vortex emanating from the inboard section of the wing is turned (fig. 4). The two vortices appear to merge and trail off the wing slightly outboard of the inboard end of the chord-extension. As discussed in reference 2, this turning of the leading-edge vortex undoubtedly results in a decrease in lift

at the tip sections, and although the effect is destabilizing, the C_m characteristics become more linear. (Compare figs. 6 and 8 and figs. 7 and 9.)

As the angle of attack is increased, the leading-edge vortex emanating from the apex of the wing apparently becomes stronger than the vortex emanating from the chord-extensions. The resultant flow tends to move outboard. It is interesting to note that at higher angles of attack (from $\alpha = 16^\circ$) the location of the resultant flow approaches that obtained for the plain wing configuration (fig. 4(j)). In like manner the pitching-moment characteristics approach those obtained with the plain wing configuration.

A secondary vortex is evident along the leading edge of the chord-extension (figs. 4(e) to 4(l)). This vortex does not appear to change in size or direction with an increase in angle of attack up to maximum lift (approximately $\alpha = 24^\circ$).

While these visual-flow studies were being made, it became apparent that to know the location of the rearward point of attachment of the vortex would be as important as to know the location of the forward portion. As a result, the wing was set at $\alpha = 10^\circ$, and a series of solution releases was made at various spanwise and chordwise positions as shown in figure 5. The dotted line superimposed on the photograph approximates the location of the rearward portion of the vortex as it passes over the wing. This procedure for locating the position and size of the vortex proved very satisfactory and, had time permitted, more studies with this technique would have been made.

Forces and Moments

The value of the aileron effectiveness parameter C_{l_δ} of the 0.495-semispan aileron is 0.00085 for the plain wing at zero lift (fig. 14) and is in accordance with that estimated by simple sweep theory (ref. 4). Throughout the low angle-of-attack range (up to approximately $C_L = 0.4$), the value of C_{l_δ} varies only slightly (fig. 14) despite significant flow changes which produce large changes in pitching-moment coefficient C_m. At $\alpha = 10^\circ$, where the leading-edge vortex has broken away from the leading edge of the tip section and where it apparently is leaving the wing inboard of the tip of the aileron, no appreciable change can be noted in C_{l_δ} (figs. 4(f) and 5). The same can be said for the configurations with chord-extensions and with extensible leading-edge flaps. Although the leading-edge vortex is turned away from the tip at very low values of α and the vortex apparently leaves the wing over the aileron, no appreciable change in the value of C_{l_δ} from that for the plain wing configuration can be noted.

It was felt that the outboard portion of the aileron, which was apparently in a region of mixed flow, was partly responsible for the ineffectiveness of the aileron in the moderate and high angle-of-attack range. A decision was made to test an inboard aileron. However, because of model construction, it was not possible to move the aileron inboard, but the outboard 25 percent of the aileron could be fixed to the wing. This resulted in a more centrally located aileron of 0.370 semispan. This configuration was tested on the plain wing and on the wing with chord-extensions and with extensible leading-edge flaps. The values of C_{l_δ} obtained for the three configurations were essentially the same; the value of C_{l_δ} was 0.00063, or approximately 30 percent less than that obtained with the 0.495-semispan aileron. As in the case of the 0.495-semispan aileron, the value of C_{l_δ} obtained with the 0.370-semispan aileron for the plain wing at zero lift was in accordance with that value estimated from reference 4. Application of a correction for the geometric differences between the two aileron spans tested, $\frac{(C_{l_\delta})_{0.495}}{Q_{0.495}/Q_{0.370}}$, to the data for the 0.495-semispan aileron gave results comparable to those obtained with the 0.370-semispan aileron (fig. 14). This would tend to indicate that the differences between the two sets of aileron data were due to geometric rather than aerodynamic characteristics.

It is interesting to note that at higher negative deflections ($\delta_a = -20^\circ$ and -25°) for the 0.495 semispan aileron on the plain wing configuration, a loss in C_l occurs (fig. 7) when the leading-edge vortex first appears. A recovery in C_l was noted when the leading edge of the vortex left the leading edge of the tip section and moved inboard (fig. 4(f)). As the angle of attack was increased the loss in C_l followed the same trend for all the deflections. With the addition of chord-extensions and extensible leading-edge flaps, (figs. 9 and 11) it may be noted that the initial loss of C_l as described for the plain wing configuration was eliminated. However, as the angle of attack was increased, the resultant vortex formed by the vortices emanating from the apex of the wing and of the chord-extension begins to move outboard (until it approaches the path taken by the vortex of the plain wing). The loss in C_l becomes similar to that obtained for the plain wing configuration. With the 0.370-semispan aileron, the trends are similar. However, the initial loss of C_l for the plain wing configuration is somewhat less than that obtained with the 0.495-semispan aileron. It is believed that the inboard portion of the aileron (0.370-semispan) is in a more stable region of flow.

Since the vortex appears to have no appreciable effect on the aileron effectiveness, whether a 0.495- or a 0.370-semispan aileron is used, it is believed that the trailing-edge outflow common to swept wings is the primary influence on the aileron characteristics.

CONCLUDING REMARKS

The results of an investigation of the lateral control characteristics of a 52° sweptback wing having an aspect ratio of 2.83 and incorporating circular-arc airfoil sections, with and without chord-extensions and extensible leading-edge flaps and equipped with either a 0.495-semispan or 0.370-semispan aileron, are summarized as follows:

The changes in pitching moment throughout the angle-of-attack range could be associated with changes in leading-edge flow. Although the leading-edge flow was markedly changed by the addition of chord-extensions, the aileron effectiveness was not materially different from that obtained on the plain wing. This was true for the wing equipped with either the 0.370- or the 0.495-semispan aileron. Yet, at very high negative aileron deflections and low angles of attack, the addition of chord-extensions did cause some change in the total rolling moment.

The values of the aileron effectiveness parameter C_{l_δ} on the plain wing at zero lift for ailerons of 0.495 and 0.370 semispan were 0.00085 and 0.00063, respectively; these values were in accordance with those estimated by simple sweep theory. However, at maximum lift the values of C_{l_δ} were approximately 65 percent of the values obtained at zero lift for each configuration. With the 0.370-semispan aileron, the value of C_{l_δ} was approximately 30 percent less at zero lift than the value obtained with the 0.495-semispan aileron. This reduction was attributed to geometric differences rather than aerodynamic differences.

Langley Aeronautical Laboratory,
National Advisory Committee for Aeronautics,
Langley Field, Va.

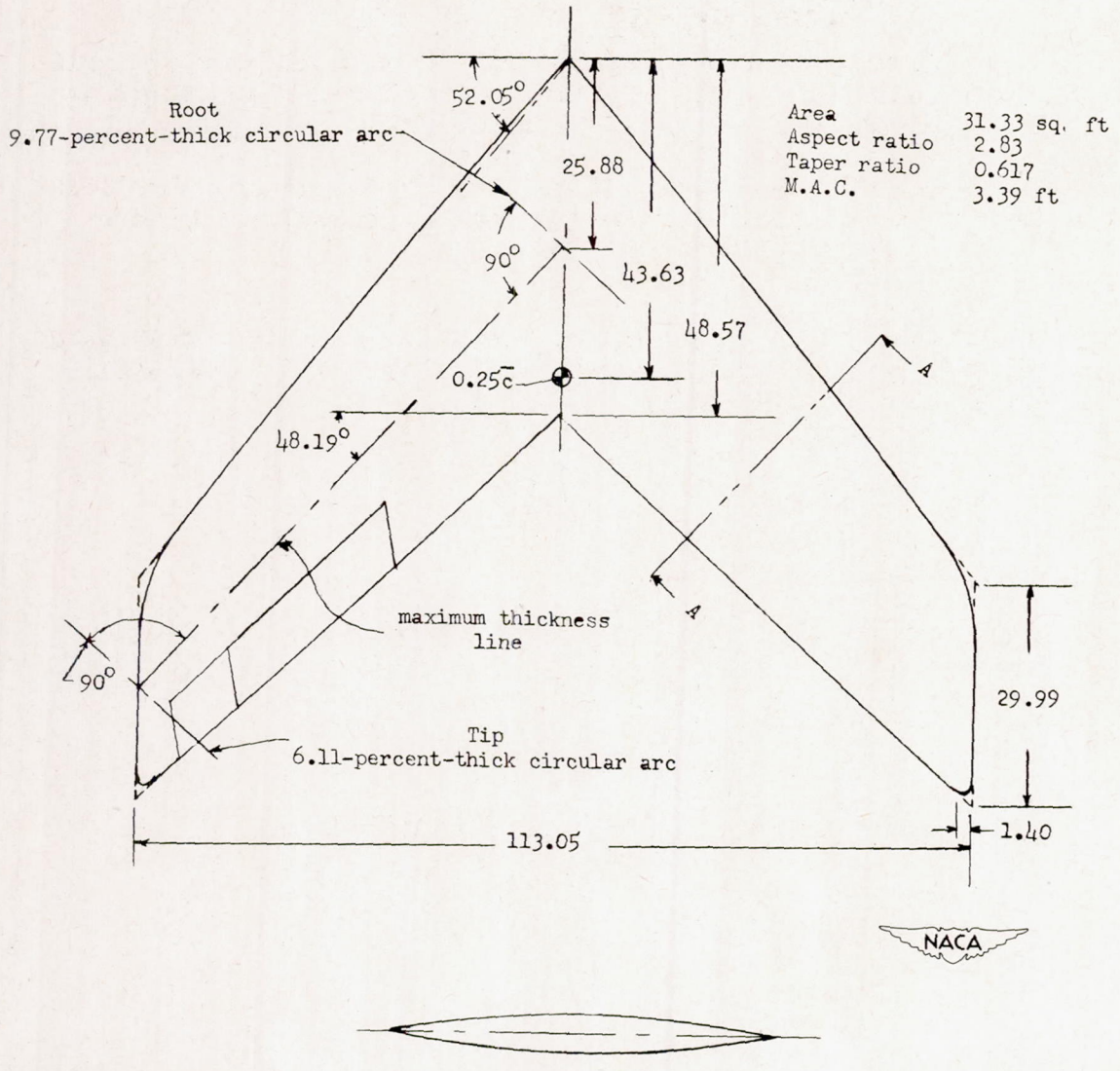
REFERENCES

1. Furlong, G. Chester: Exploratory Investigation of Leading-Edge Chord-Extensions To Improve the Longitudinal Stability Characteristics of Two 52° Sweptback Wings. NACA RM L50A30, 1950.

2. Furlong, G. Chester, and McHugh, James G.: A Summary and Analysis of the Low-Speed Longitudinal Characteristics of Swept Wings at High Reynolds Number. NACA RM L52D16, 1952.

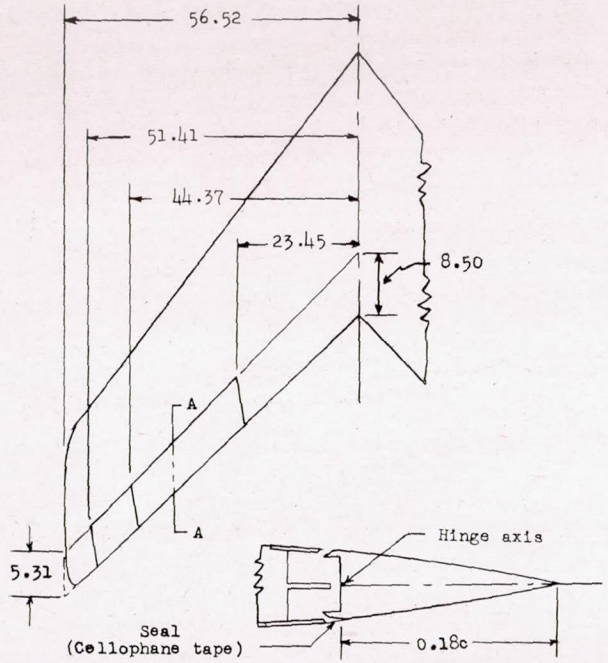
3. Sivells, James C., and Salmi, Rachel M.: Jet-Boundary Corrections for Complete and Semispan Swept Wings in Closed Circular Wind Tunnels. NACA TN 2454, 1951.

4. DeYoung, John: Theoretical Antisymmetric Span Loading for Wings of Arbitrary Plan Form at Subsonic Speeds. NACA Rep. 1056, 1951. (Supersedes NACA TN 2140.)

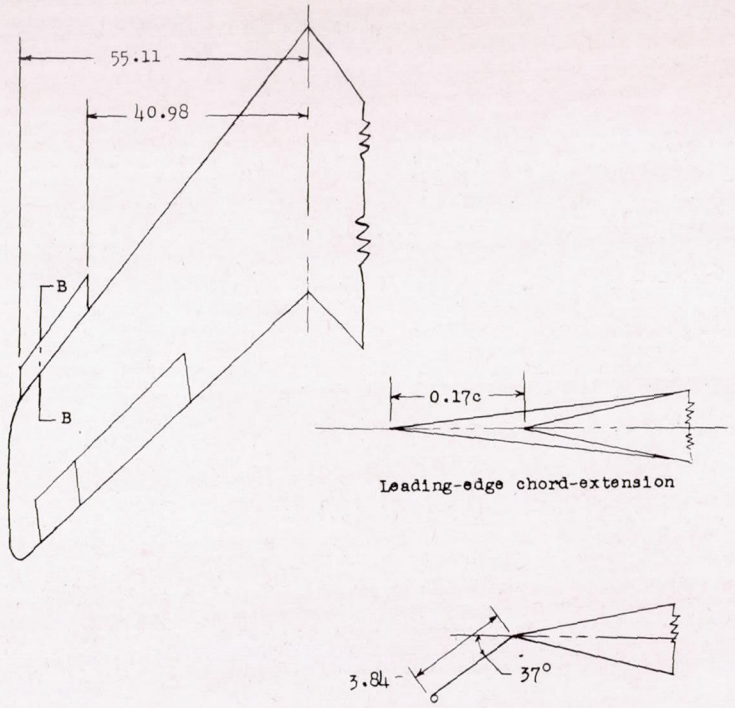


Section A-A (enlarged)

Figure 1.- Plan form of 52° sweptback wing. All dimensions are given in inches unless otherwise noted.



Section A-A (enlarged)



Leading-edge chord-extension

Leading-edge flap

Section B-B (enlarged)

Figure 2.- Details of aileron, leading-edge chord-extensions, and extensible leading-edge flaps. All dimensions are given in inches unless otherwise indicated.

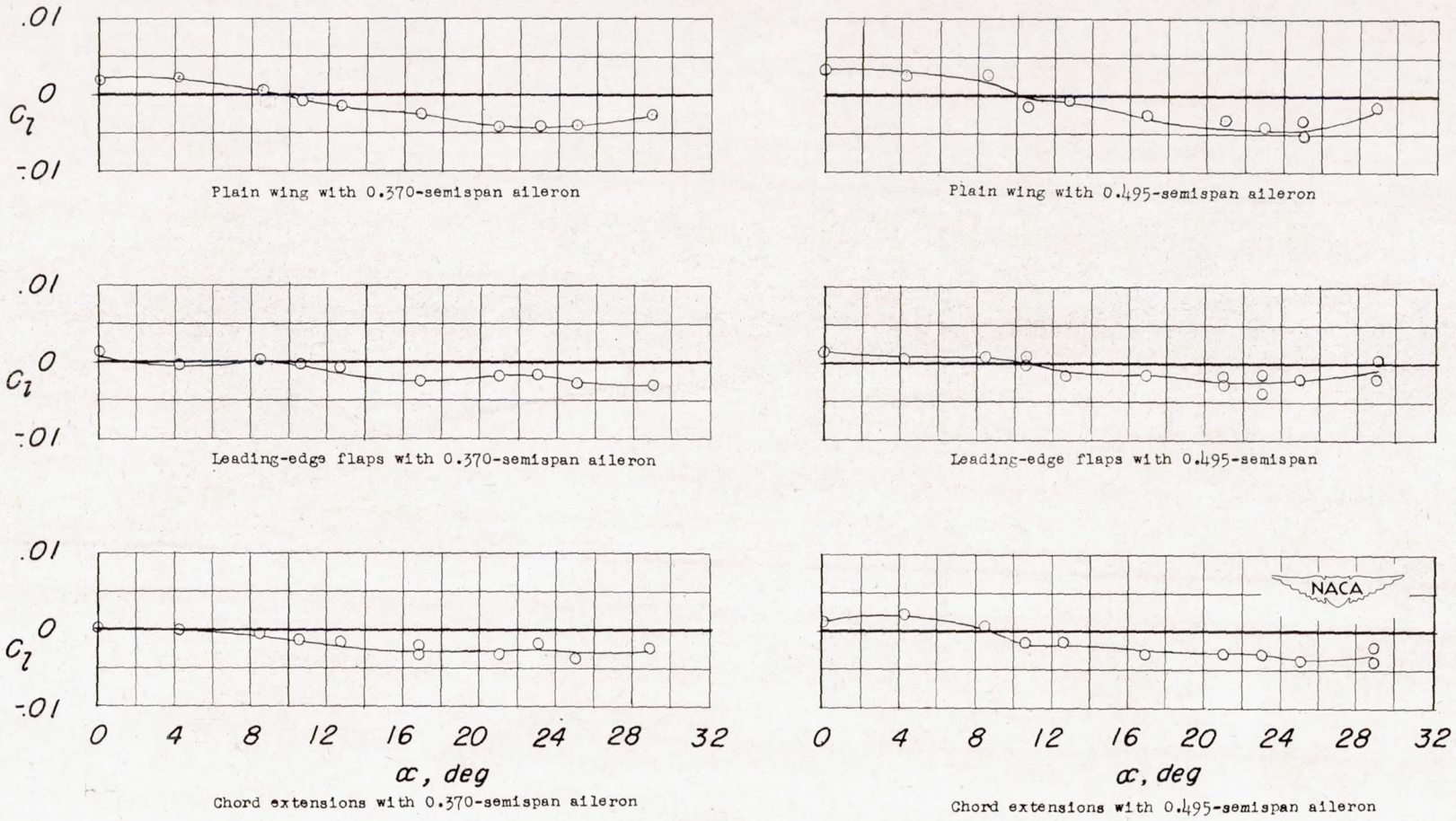
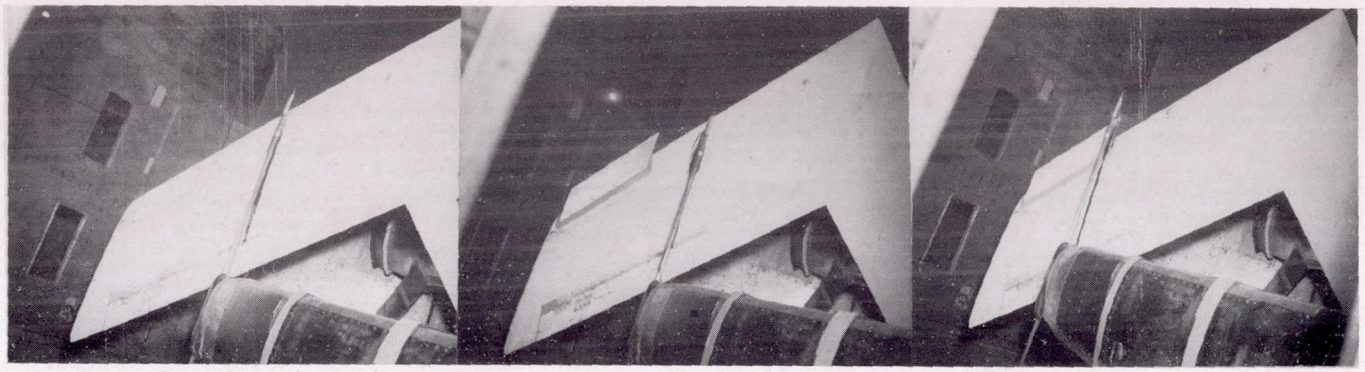
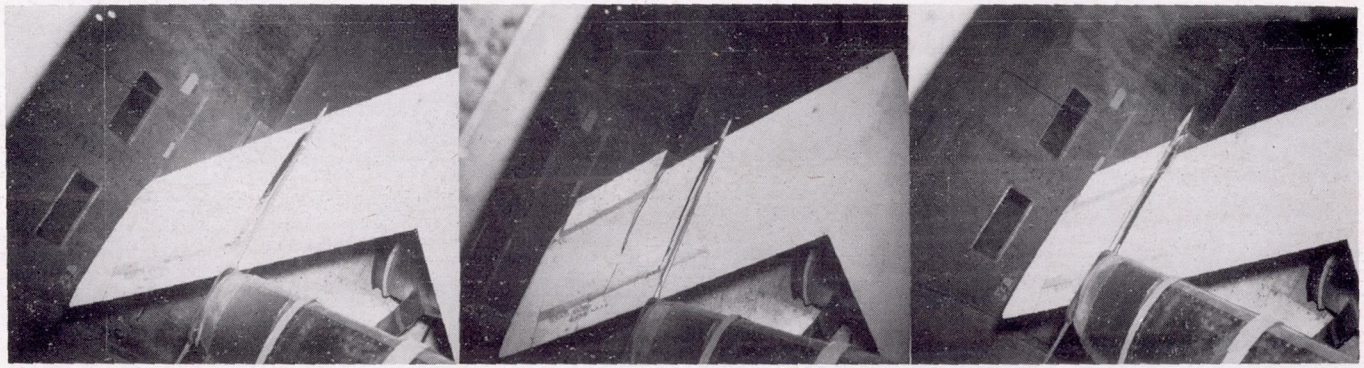


Figure 3.- Variation of rolling-moment coefficient with angle of attack at $\delta_a = 0^\circ$ for the various configurations.



(a) $\alpha = 0^{\circ}$.

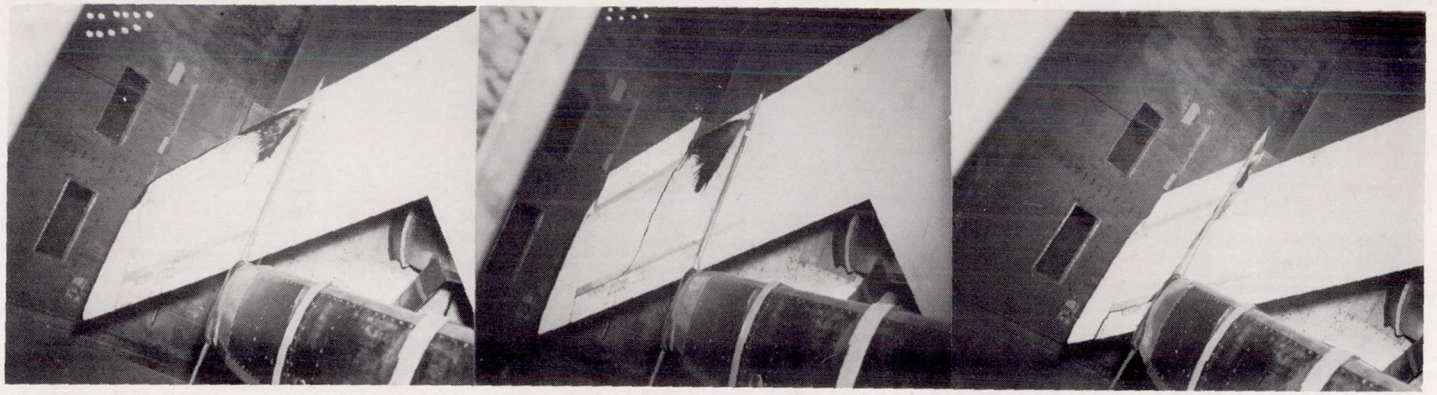


Plain wing | Wing with chord-extension | Wing with chord-extension

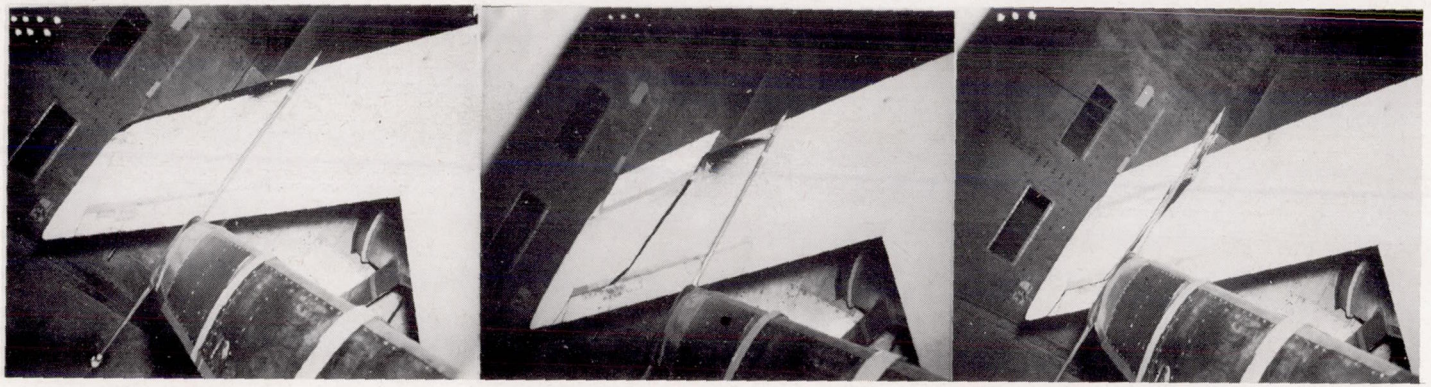
(b) $\alpha = 2^{\circ}$.

NACA L-77937

Figure 4.- Visual-flow studies on a 52° sweptback biconvex wing with circular-arc airfoil sections.



(c) $\alpha = 4^\circ$.

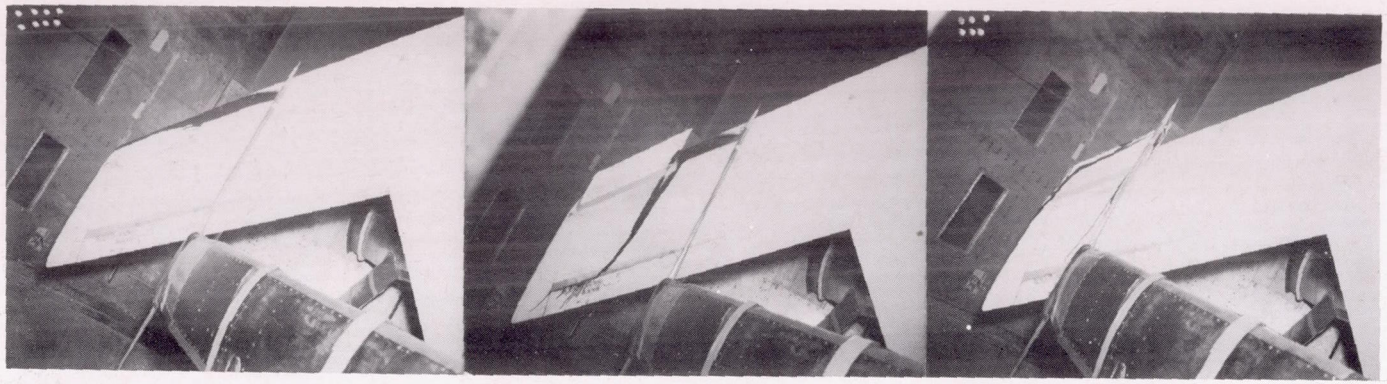


Plain wing | Wing with chord-extension | Wing with chord-extension

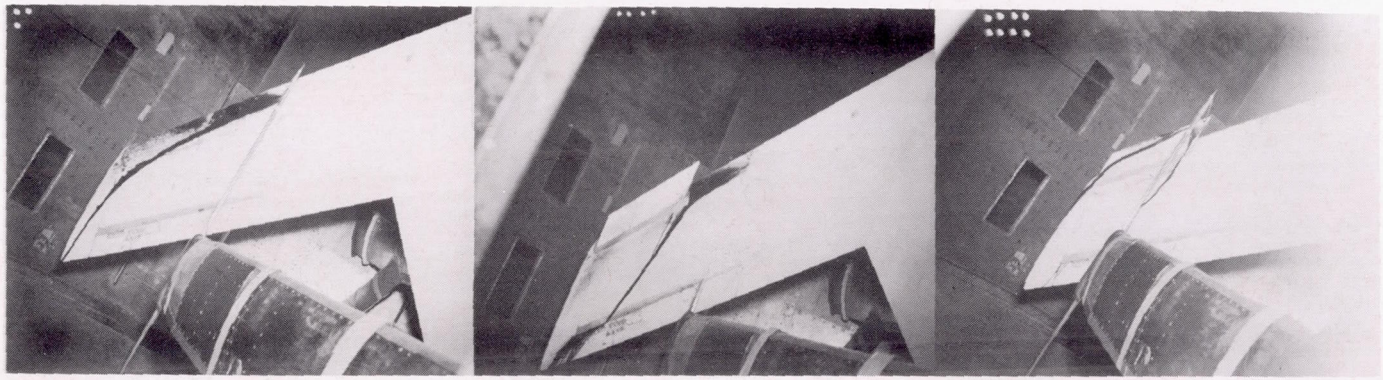
(d) $\alpha = 6^\circ$.

NACA L-77938

Figure 4.- Continued.



(e) $\alpha = 8^{\circ}$.

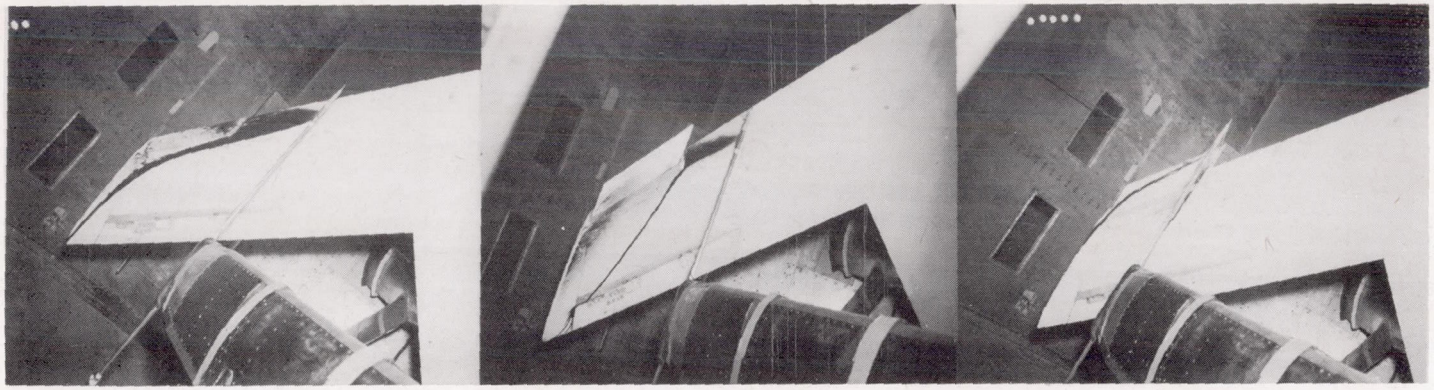


Plain wing | Wing with chord-extension | Wing with chord-extension

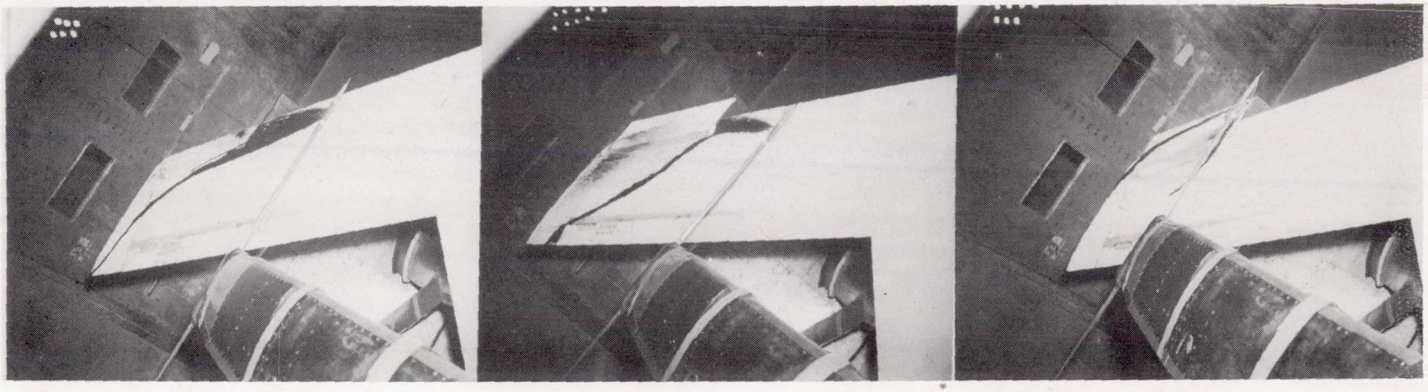
(f) $\alpha = 10^{\circ}$.

NACA L-77939

Figure 4.- Continued.



(g) $\alpha = 12^{\circ}$.

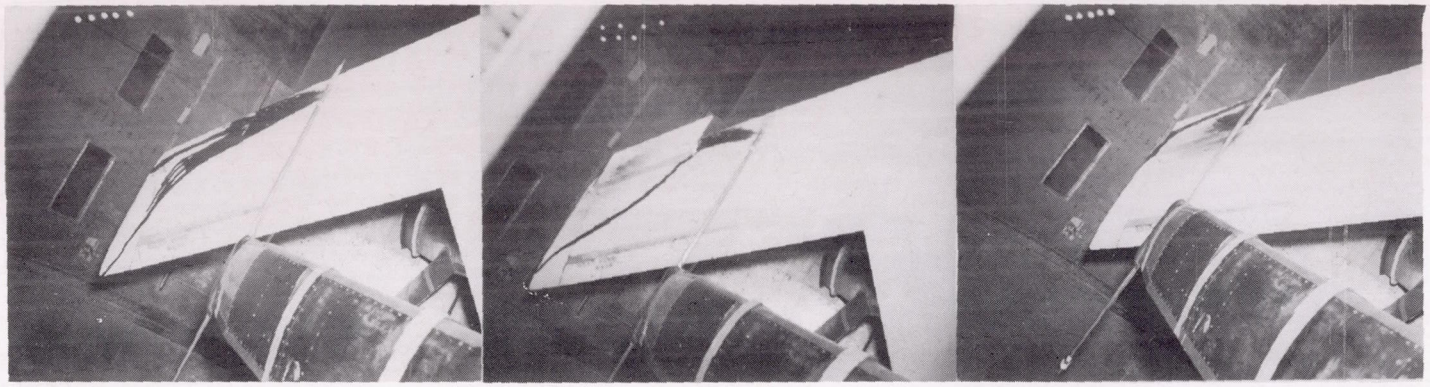


Plain wing | Wing with chord-extension | Wing with chord-extension

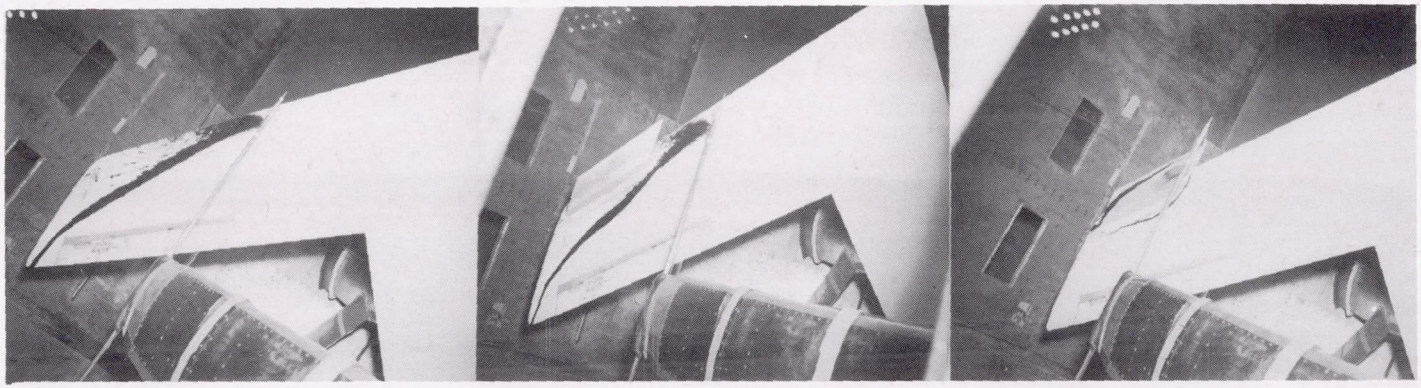
(h) $\alpha = 14^{\circ}$.

NACA L-77940

Figure 4.- Continued.



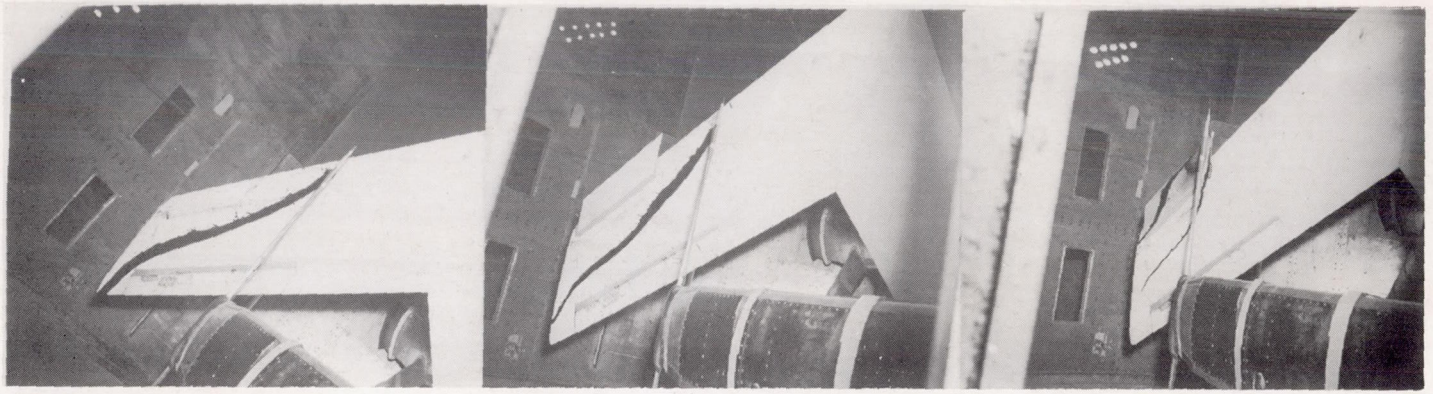
(i) $\alpha = 16^{\circ}$.



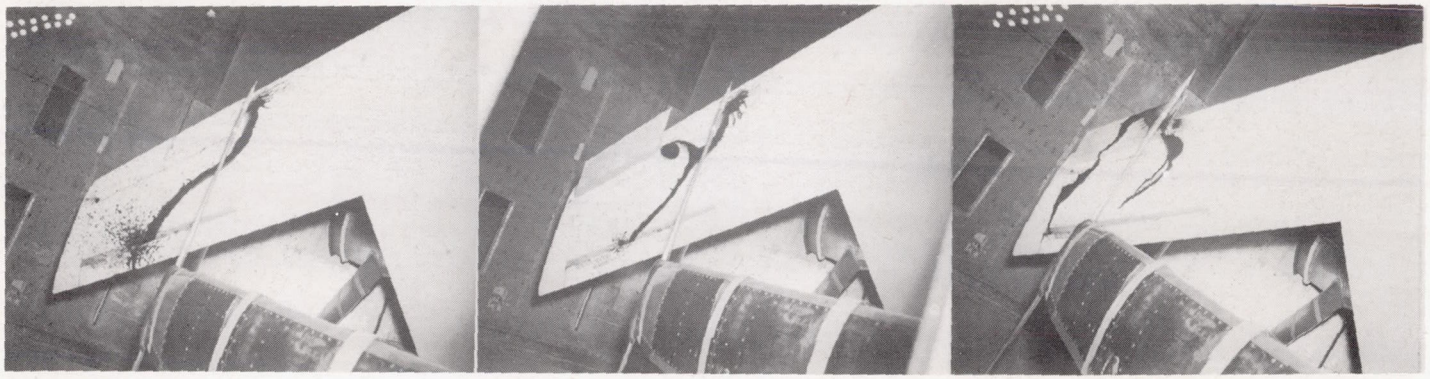
Plain wing | Wing with chord-extension | Wing with chord-extension

(j) $\alpha = 20^{\circ}$.

Figure 4.- Continued. L-77941



(k) $\alpha = 24^{\circ}$.



Plain wing | Wing with chord-extension | Wing with chord-extension

(l) $\alpha = 28^{\circ}$.

NACA L-77942

Figure 4.- Concluded.

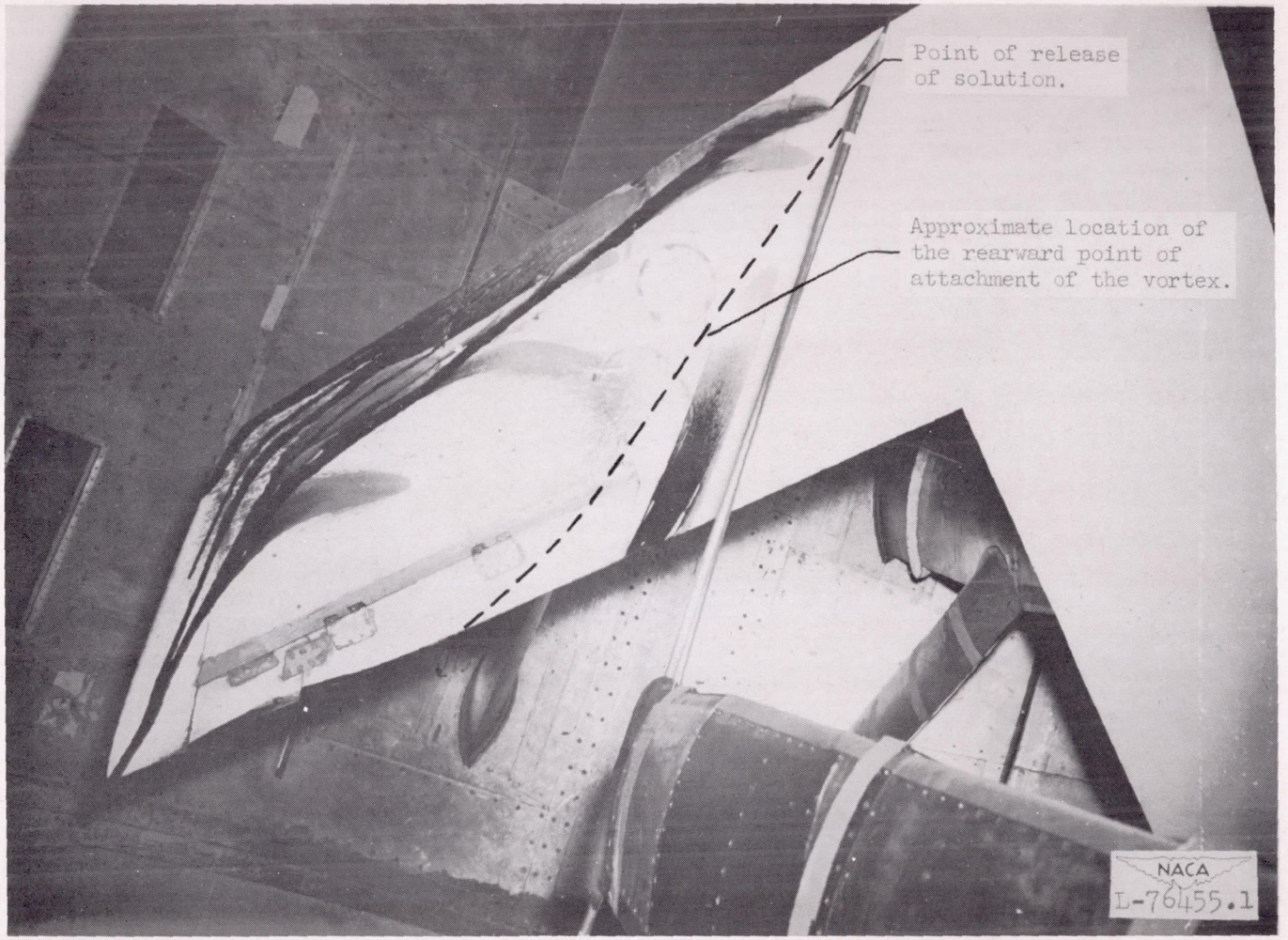
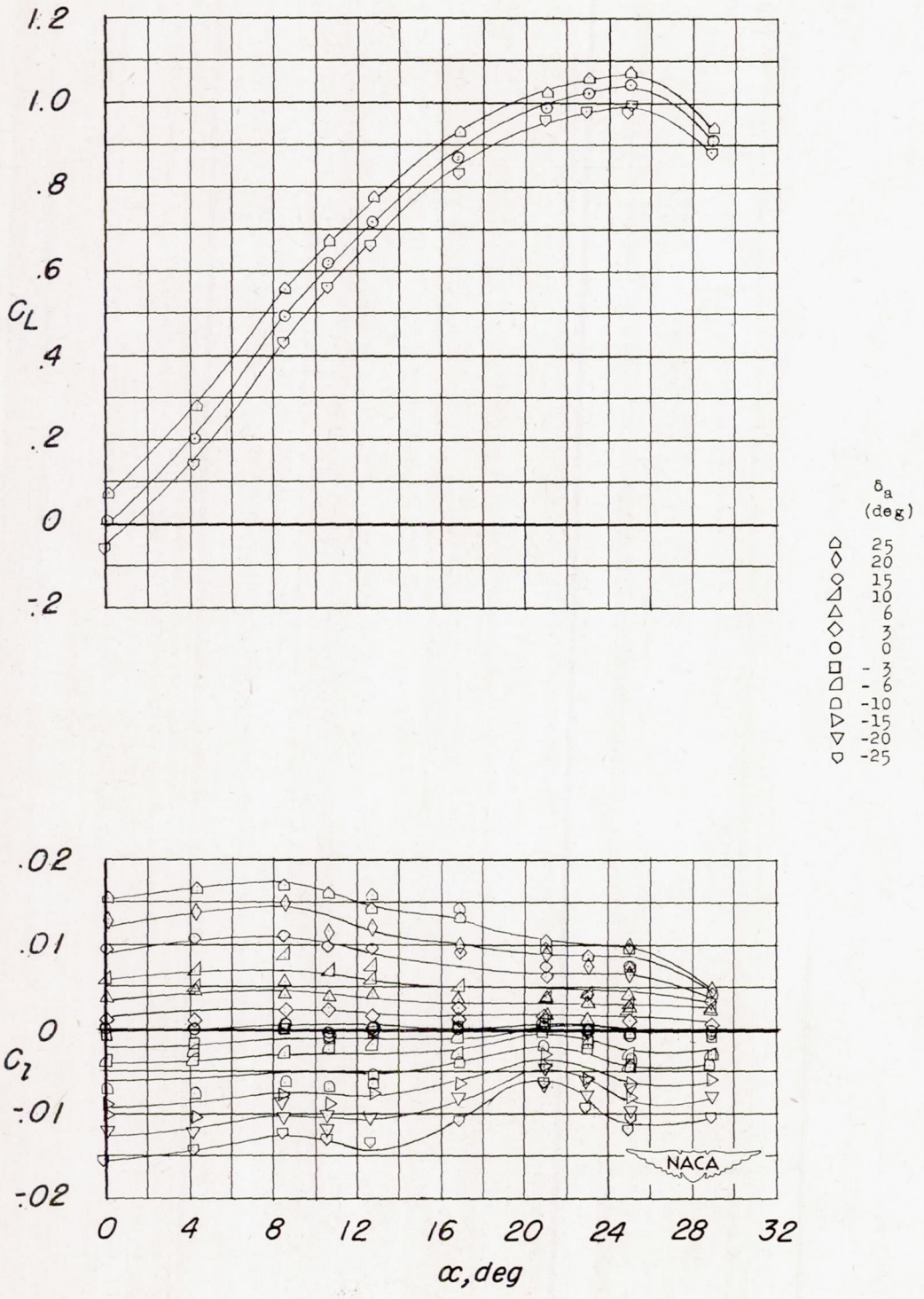
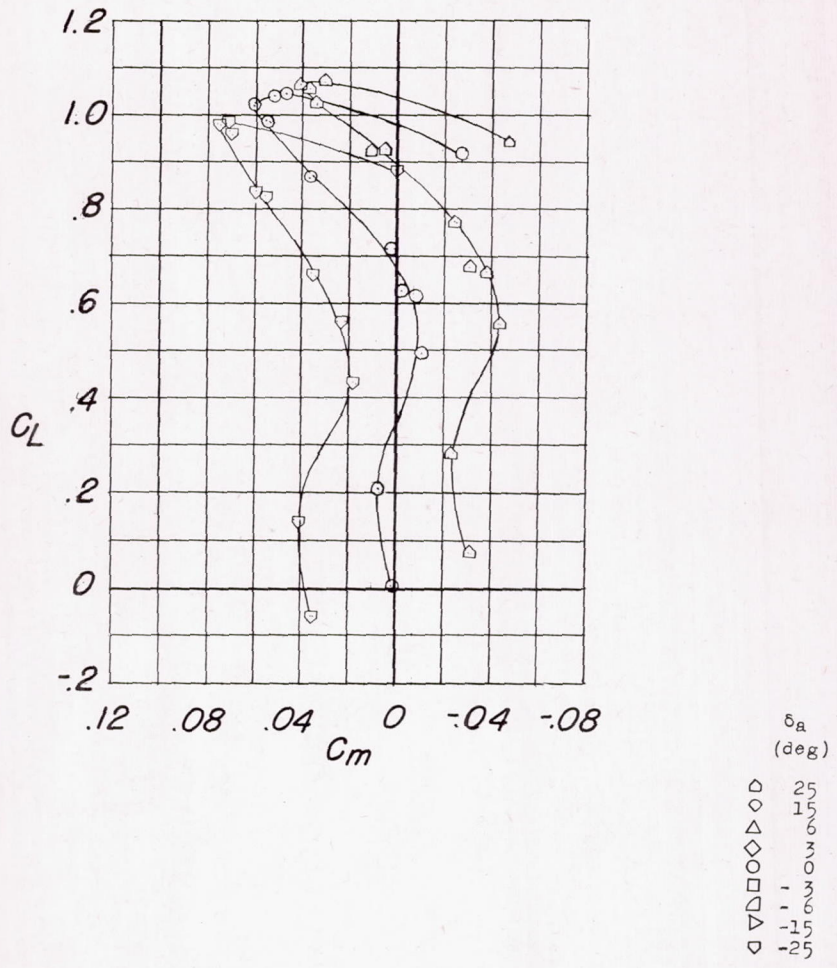


Figure 5.- Visual-flow study on a 52° sweptback biconvex wing with circular-arc airfoil sections, showing the approximate location of the rearward point of attachment of the vortex. $\alpha = 10^{\circ}$.



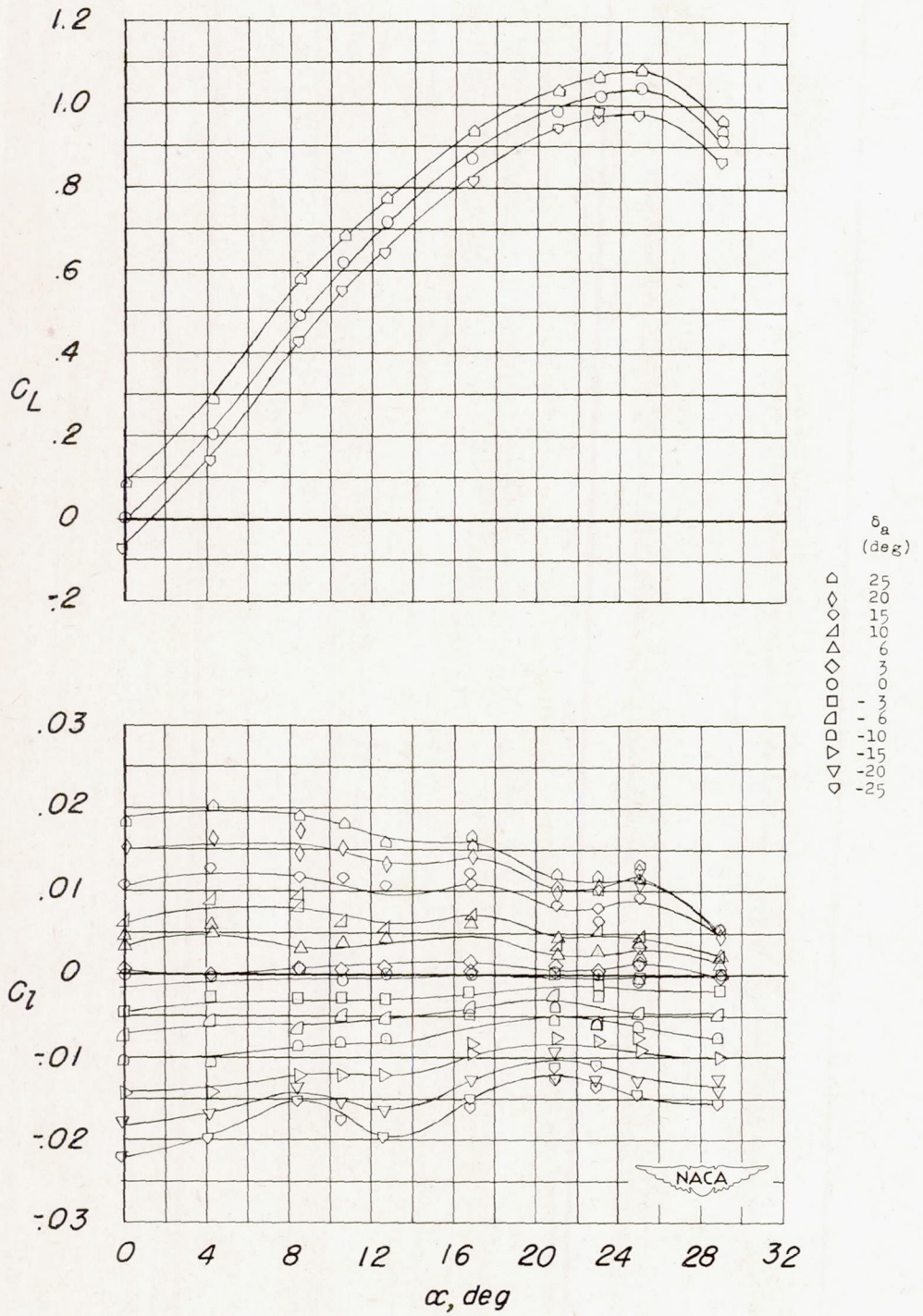
(a) Variation of C_L and C_l with α.

Figure 6.- Aileron characteristics of plain wing with 0.370-semispan aileron.



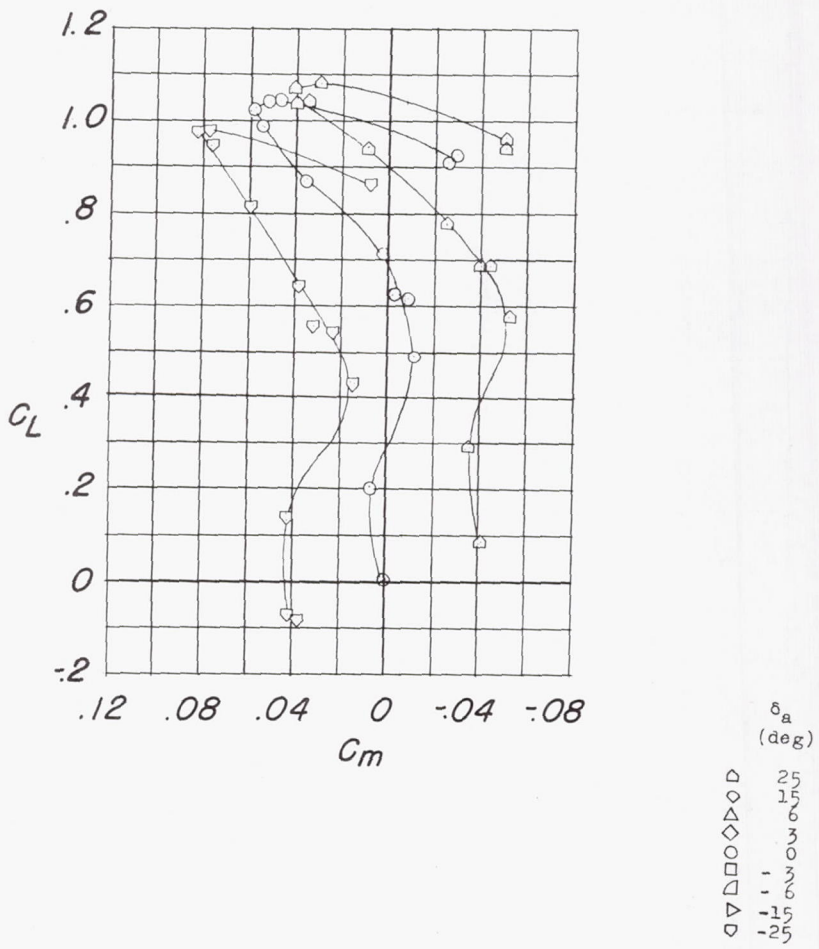
(b) Variation of C_m with C_L and C_n with α.

Figure 6.- Concluded.



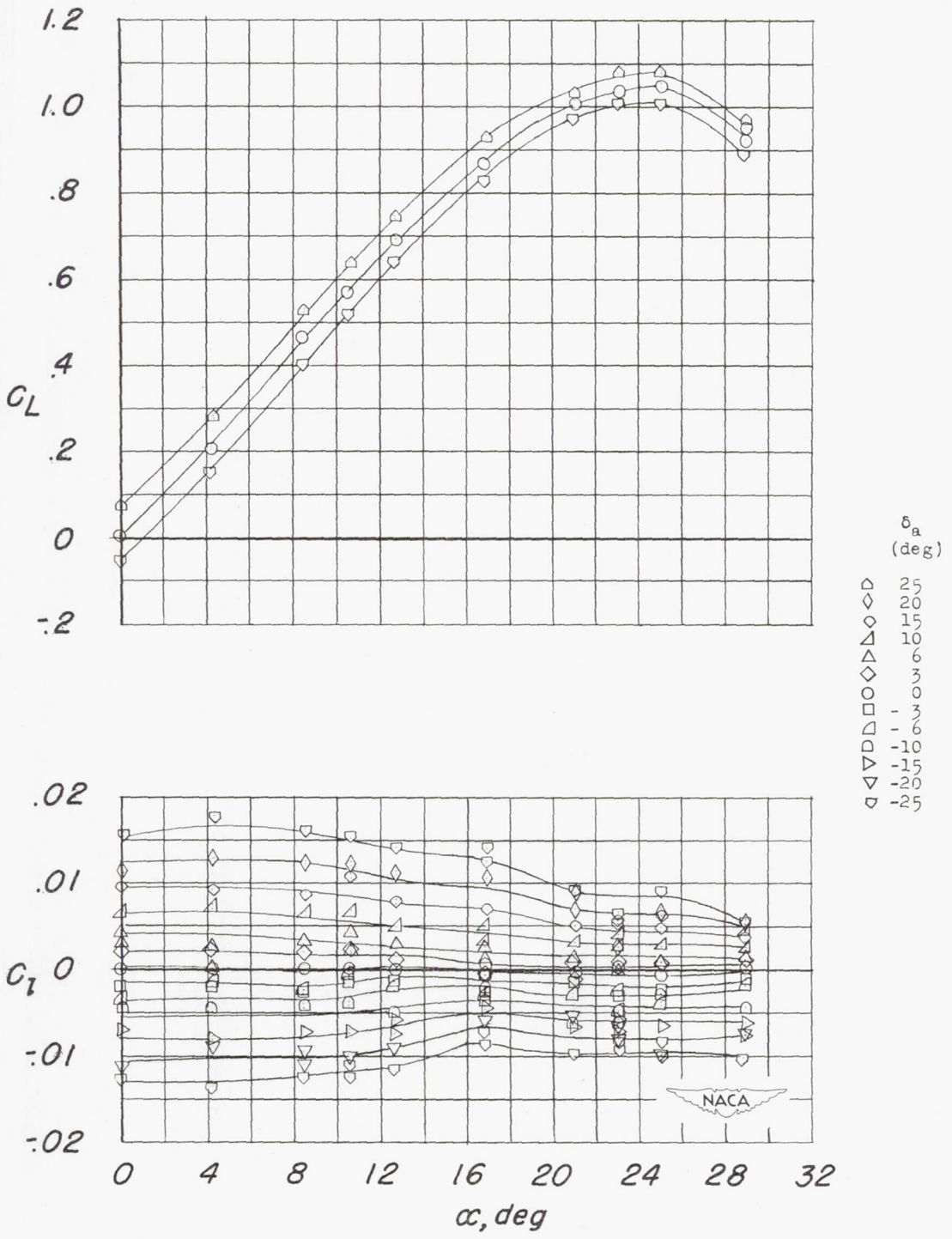
(a) Variation of C_L and C_l with α.

Figure 7.- Aileron characteristics of plain wing with 0.495-semispan aileron.



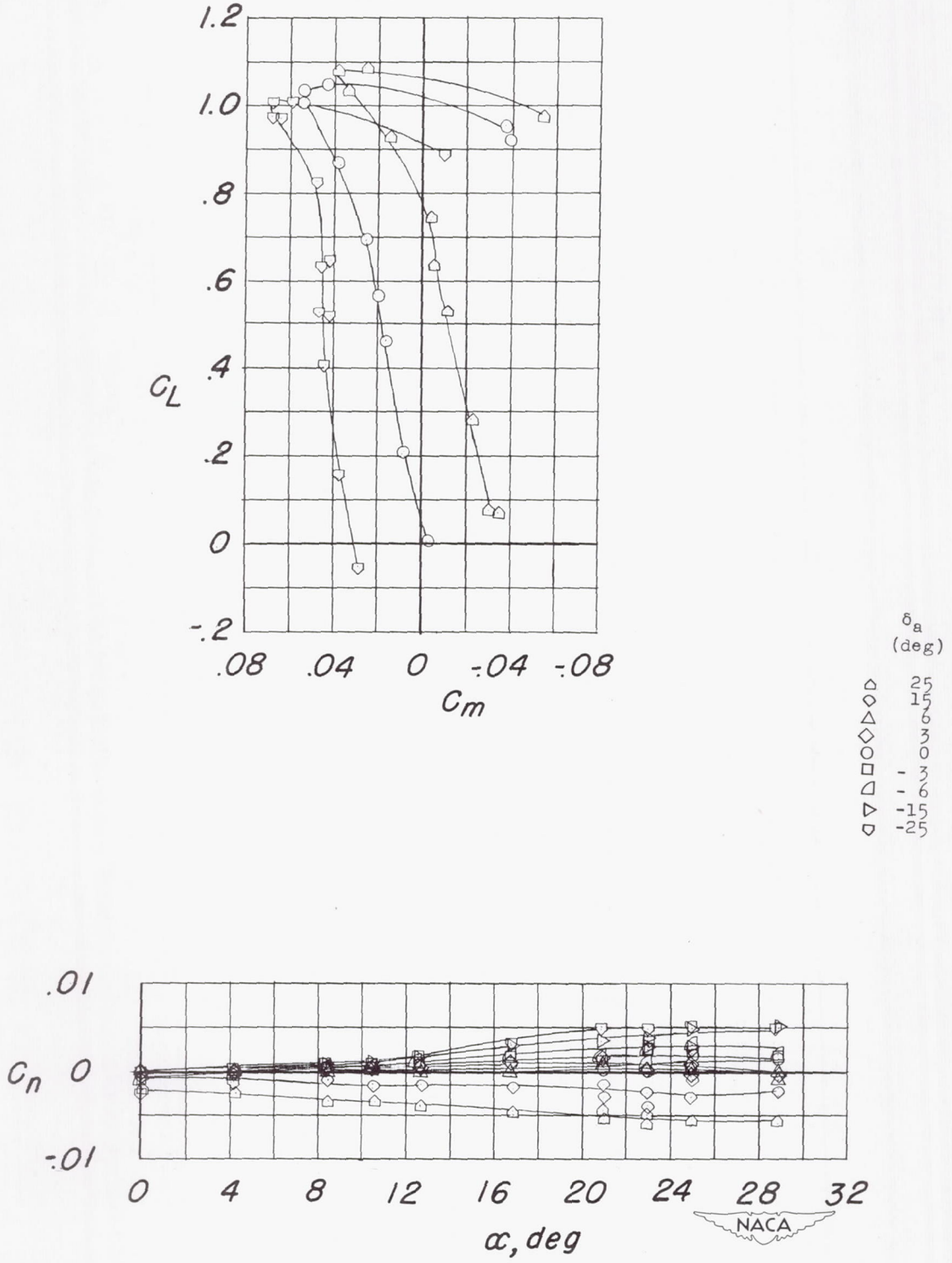
(b) Variation of C_m with C_L and C_n with α.

Figure 7.- Concluded.



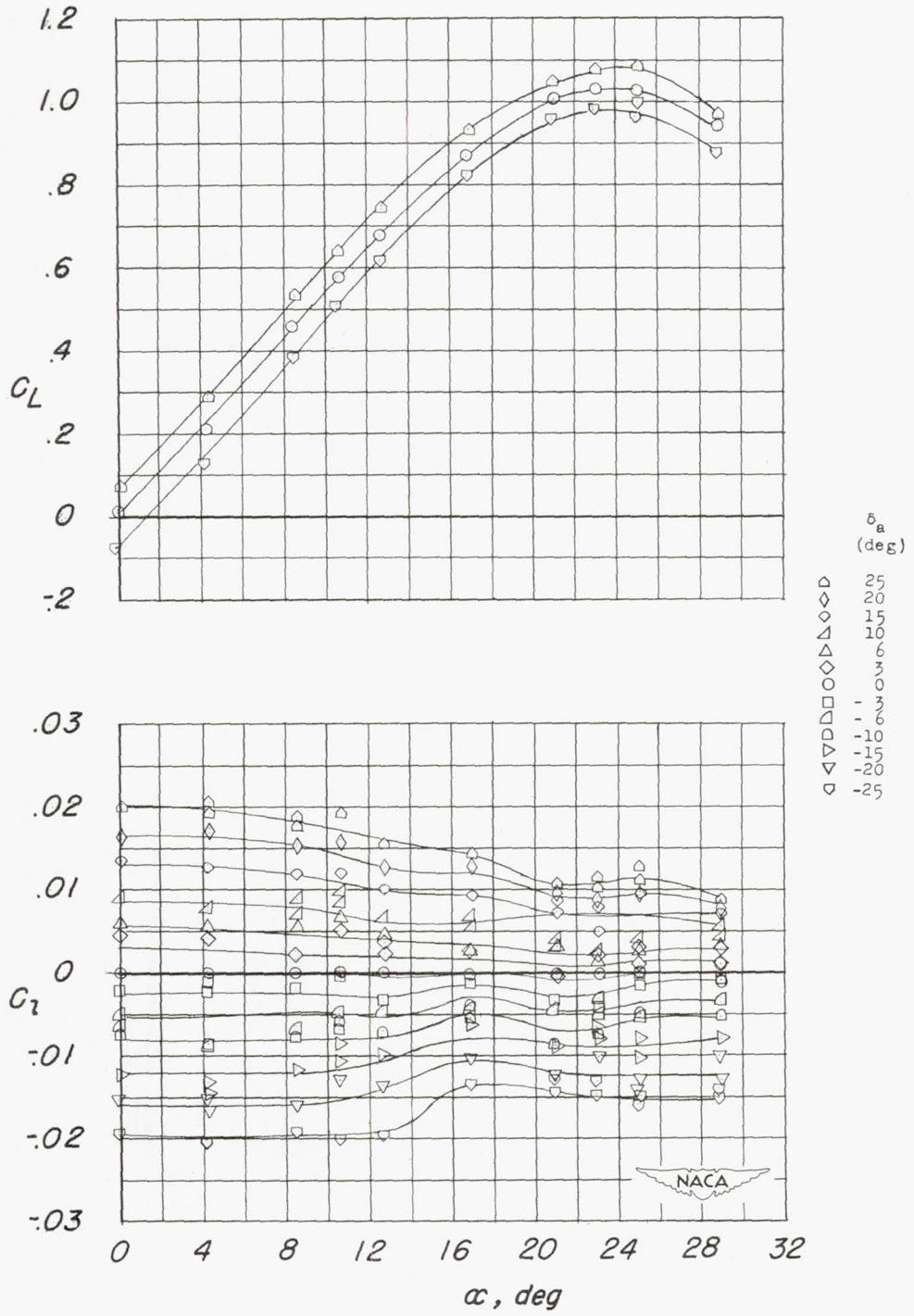
(a) Variation of C_L and C_l with α.

Figure 8.- Aileron characteristics of wing with chord-extensions and 0.370-semispan aileron.



(b) Variation of C_m with C_L and C_n with α.

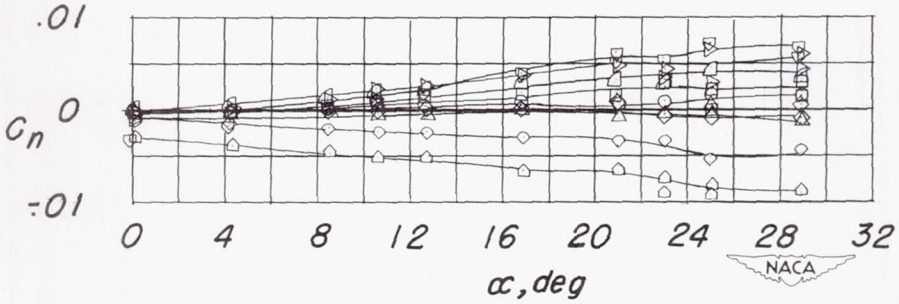
Figure 8.- Concluded.



(a) Variation of C_L and C_l with α.

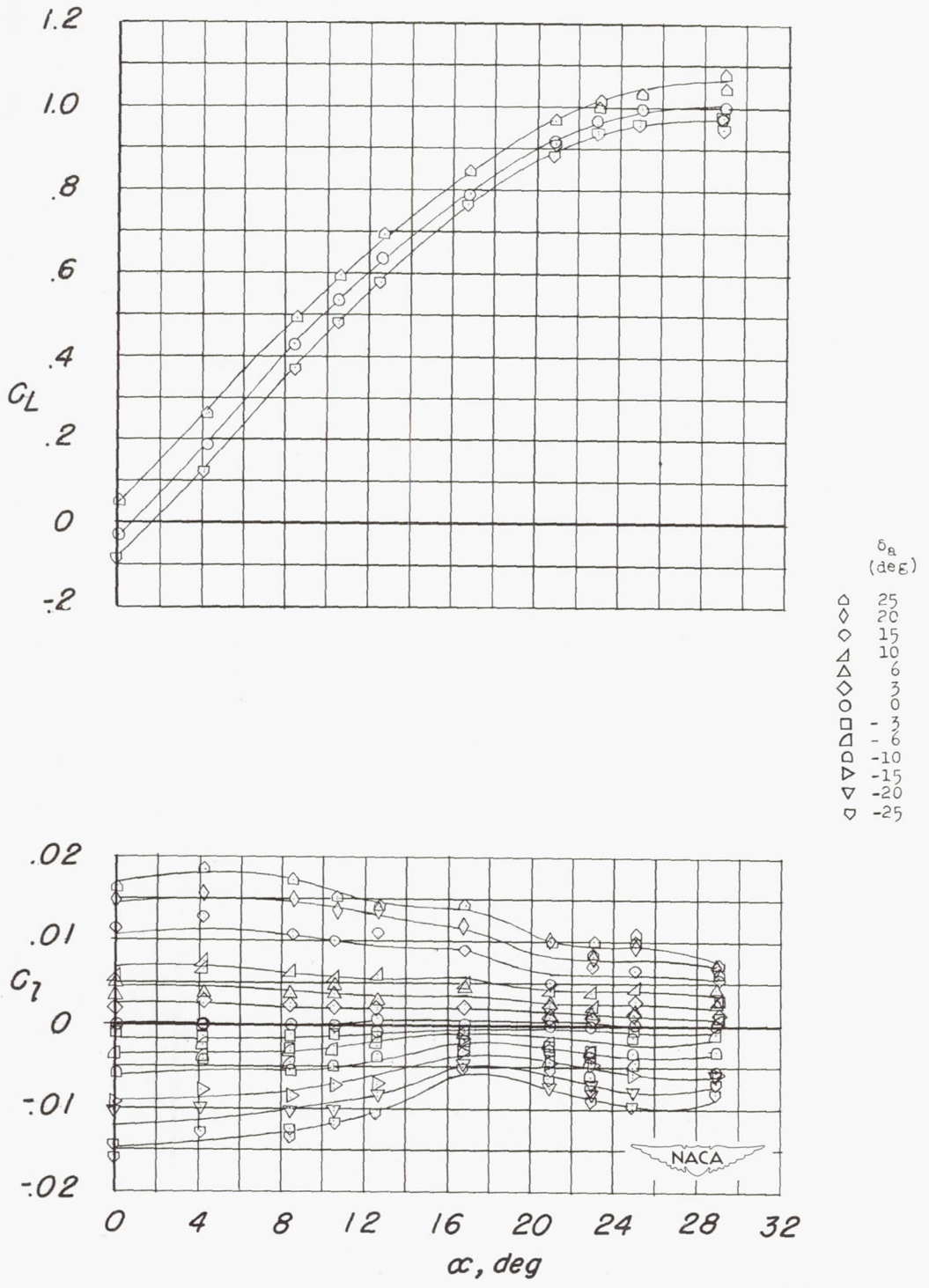
Figure 9.- Aileron characteristics of wing with chord-extensions and 0.495-semispan aileron.





(b) Variation of C_m with C_L and C_n with α.

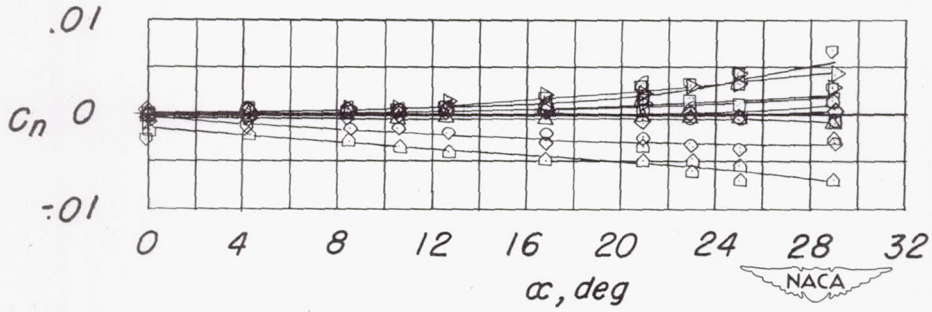
Figure 9.- Concluded.



(a) Variation of C_L and C_l with α.

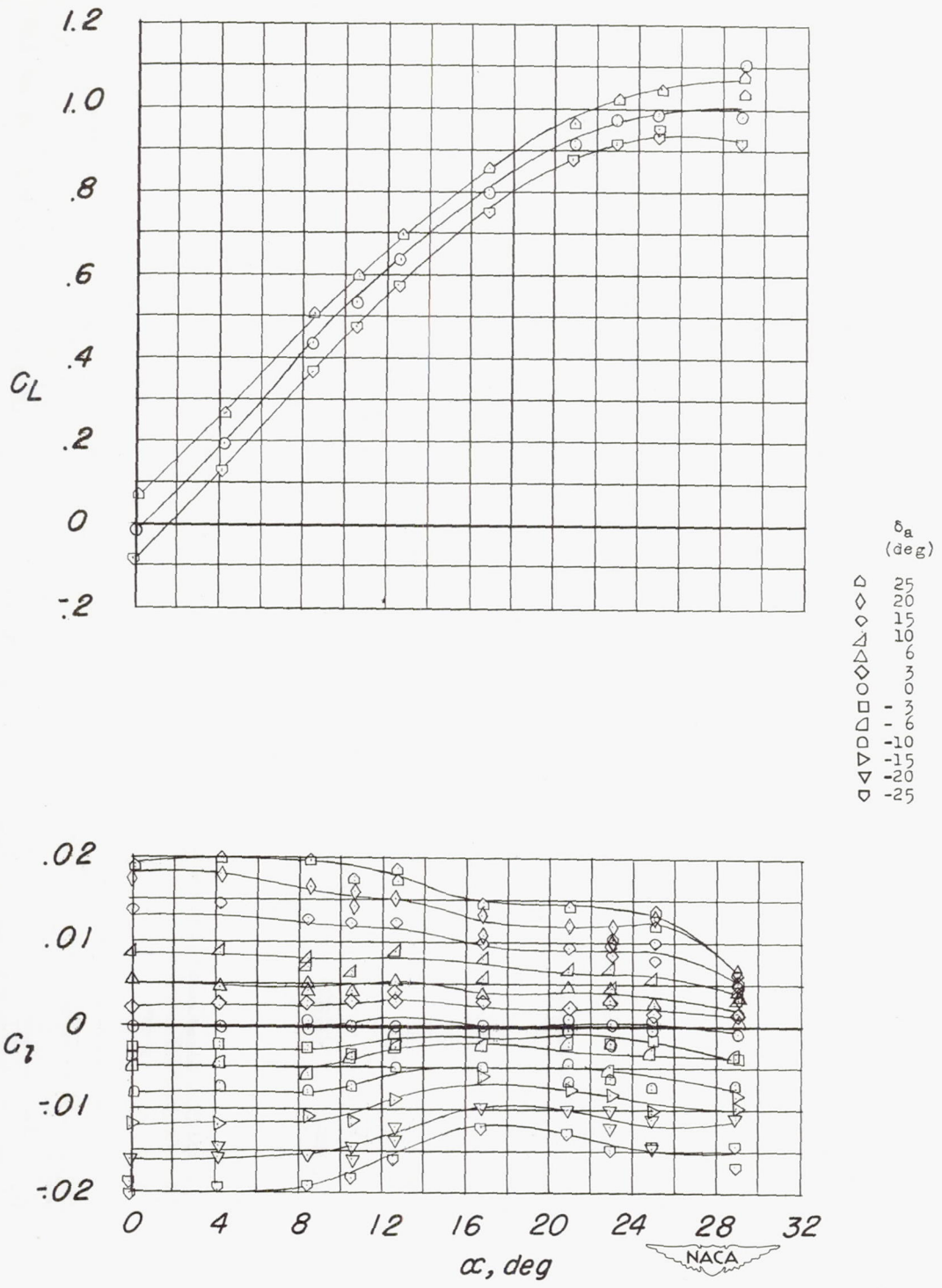
Figure 10.- Aileron characteristics of wing with extensible leading-edge flaps and 0.370-semispan aileron.





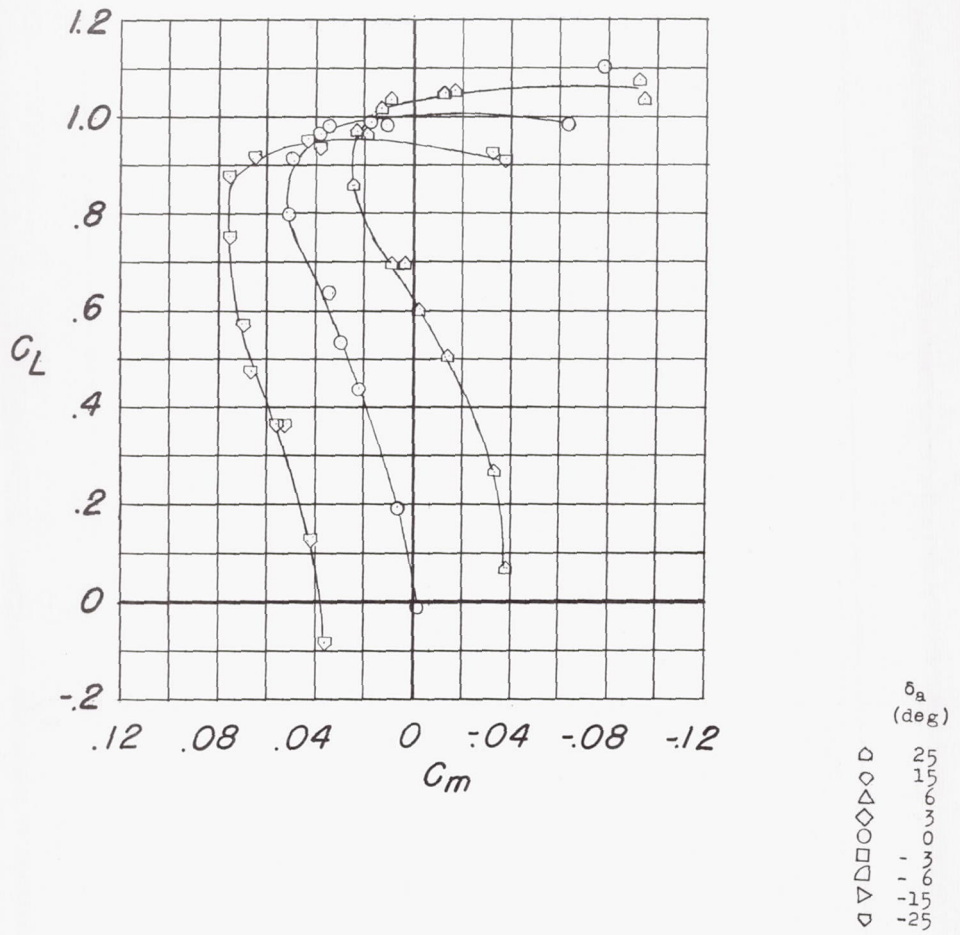
(b) Variation of C_m with C_L and C_n with α.

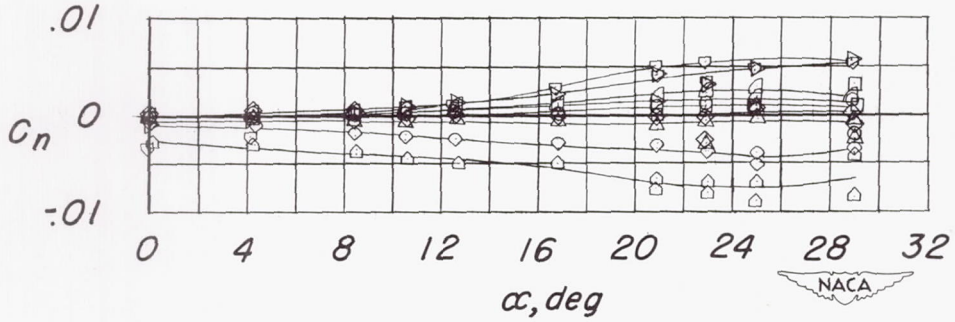
Figure 10.- Concluded.



(a) Variation of C_L and C_l with α.

Figure 11.- Aileron characteristics of wing with extensible leading-edge flaps and 0.495-semispan aileron.





(b) Variation of C_m with C_L and C_n with α.

Figure 11.- Concluded.

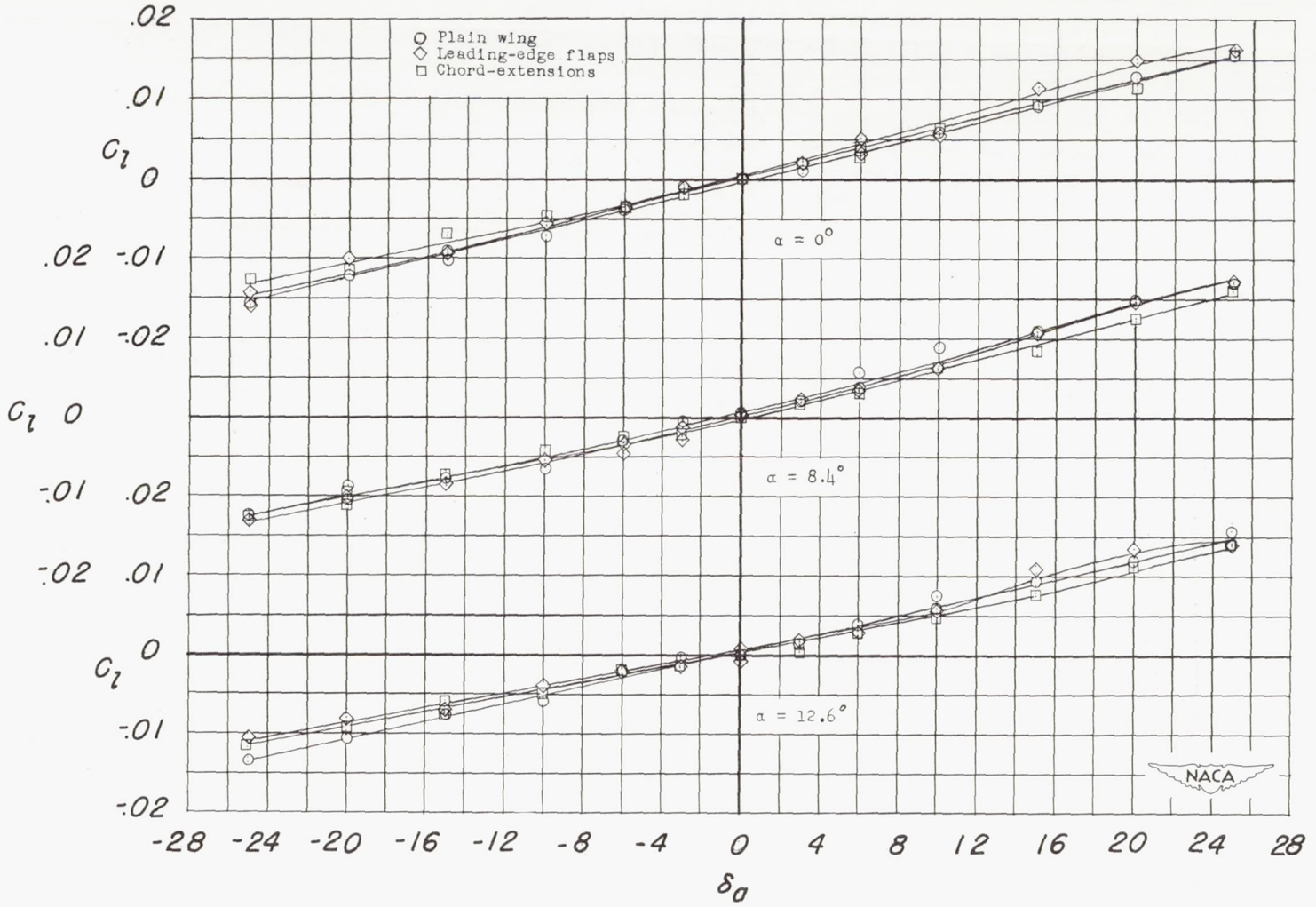


Figure 12.- The variation of rolling-moment characteristics with 0.370-semispan-aileron deflection for various model configurations and angles of attack.

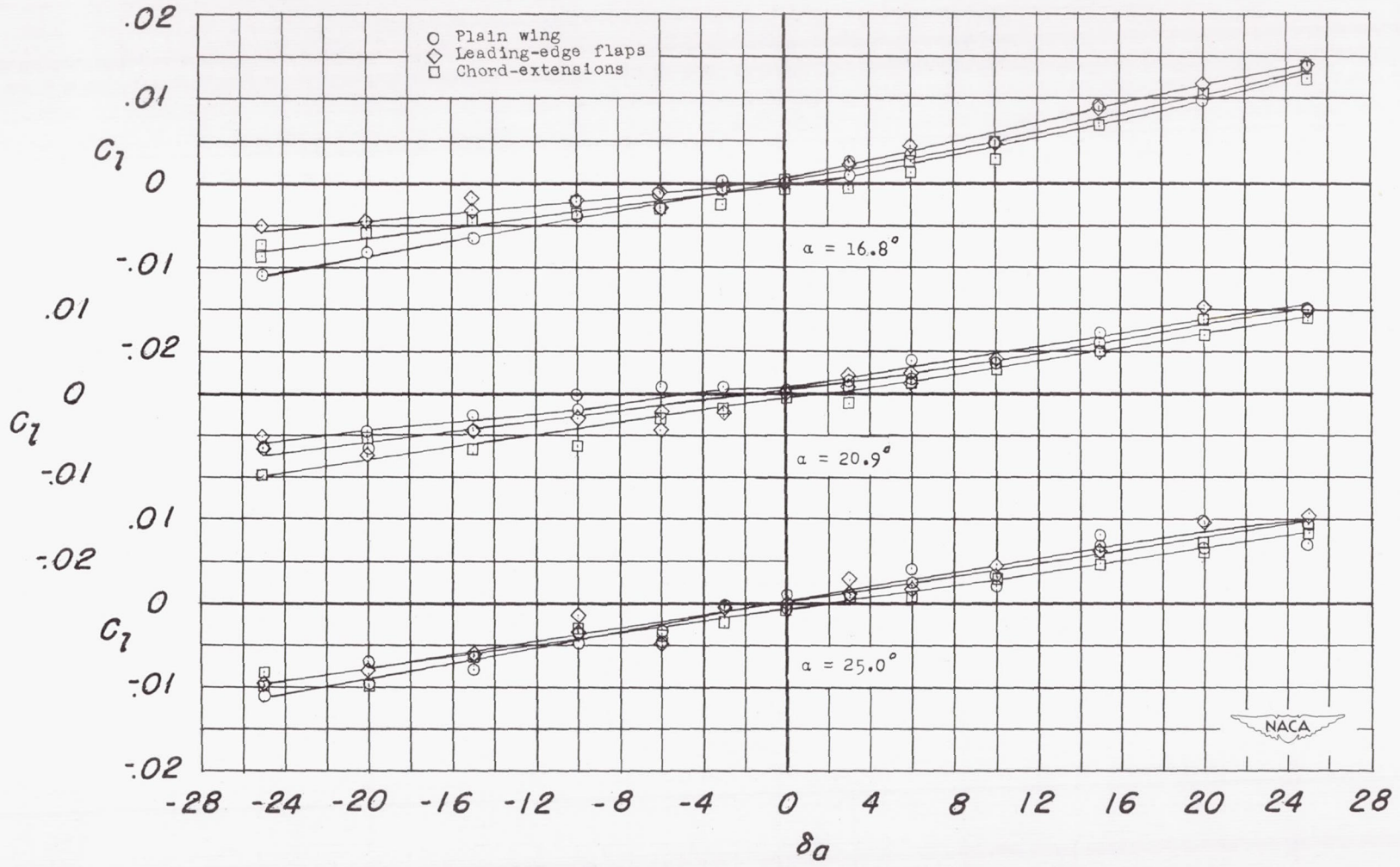


Figure 12.- Concluded.

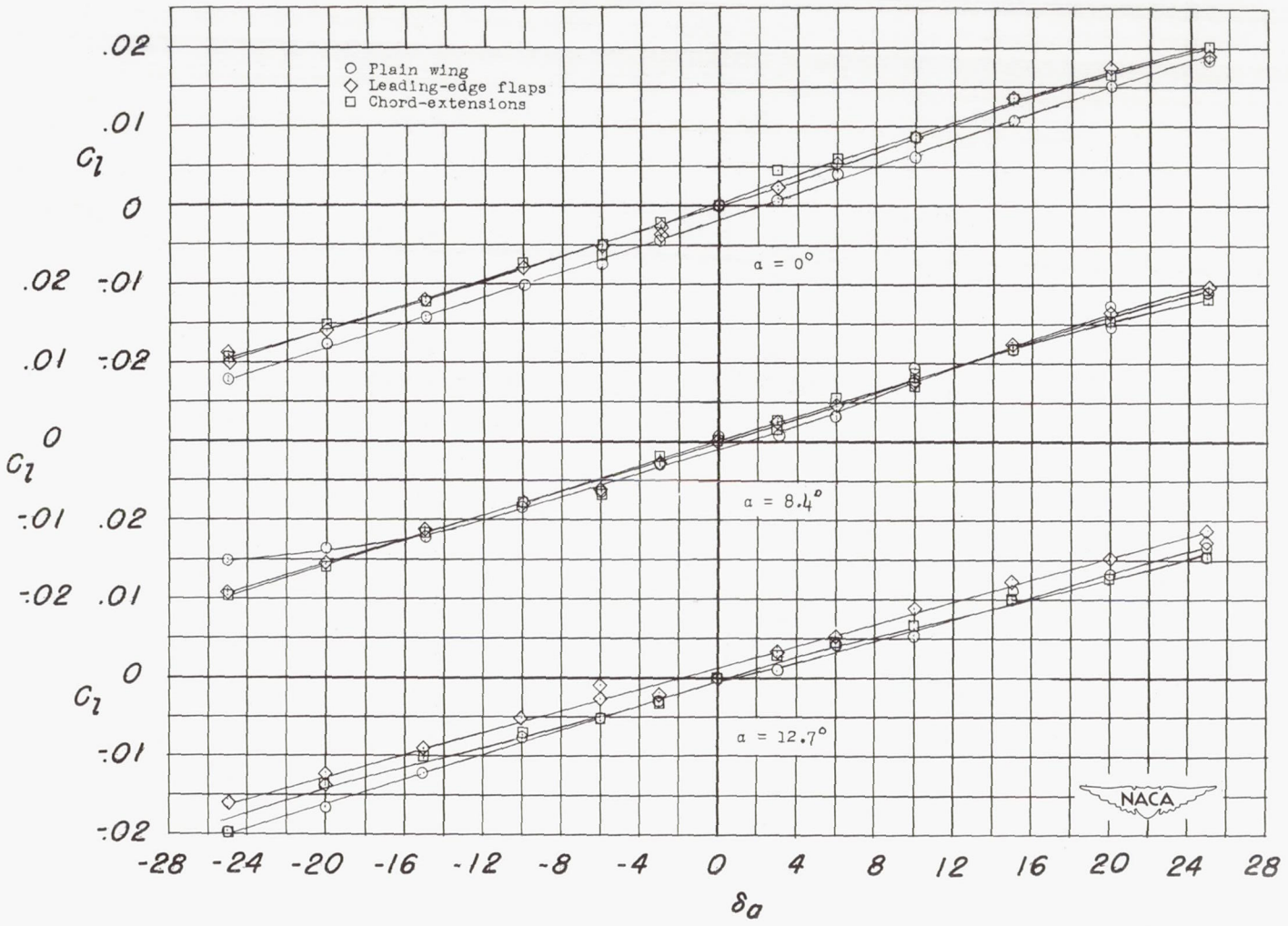


Figure 13.- The variation of rolling-moment characteristics with 0.495-semispan-aileron deflection for various model configurations and angles of attack.

CONFIDENTIAL

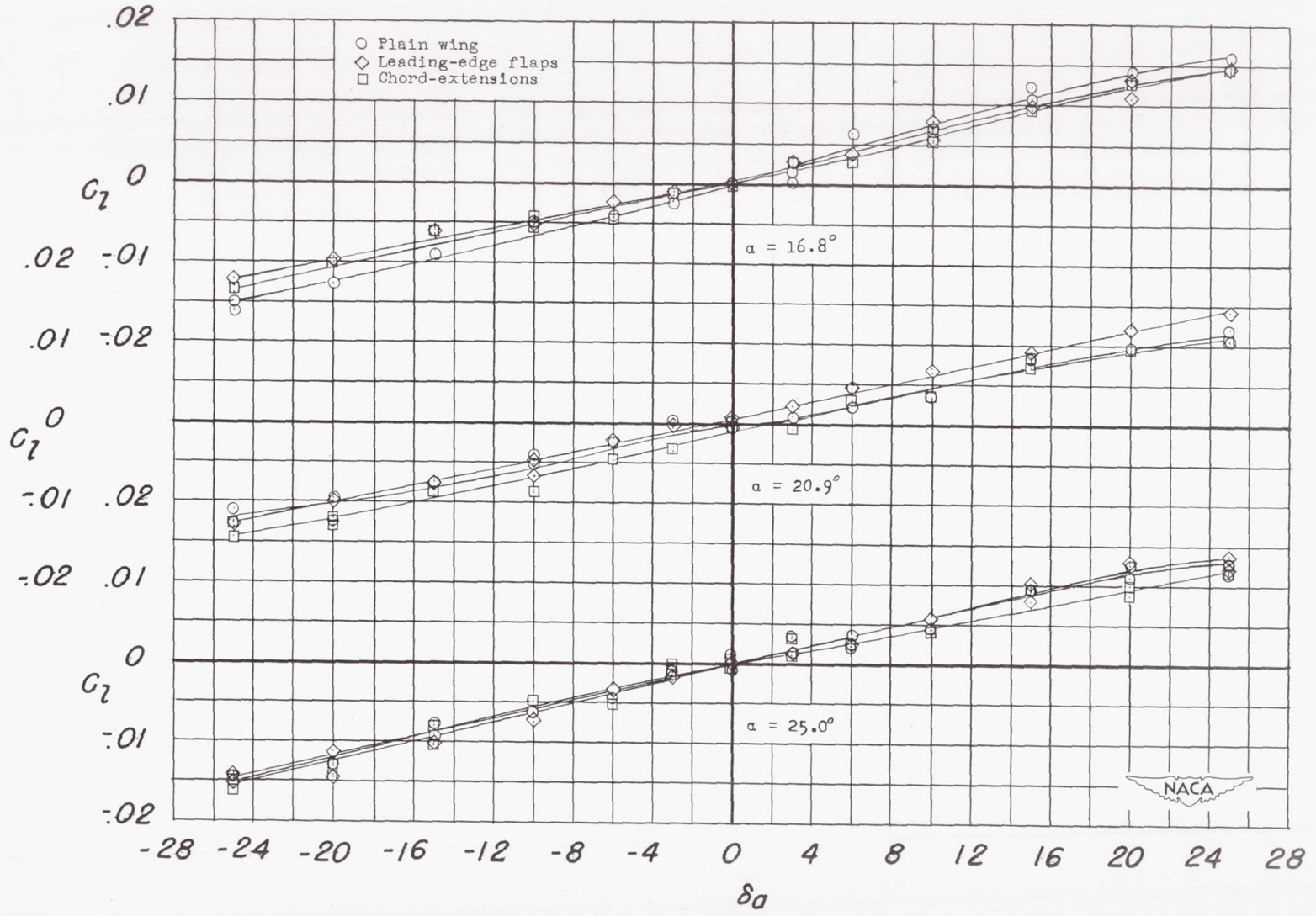


Figure 13.- Concluded.

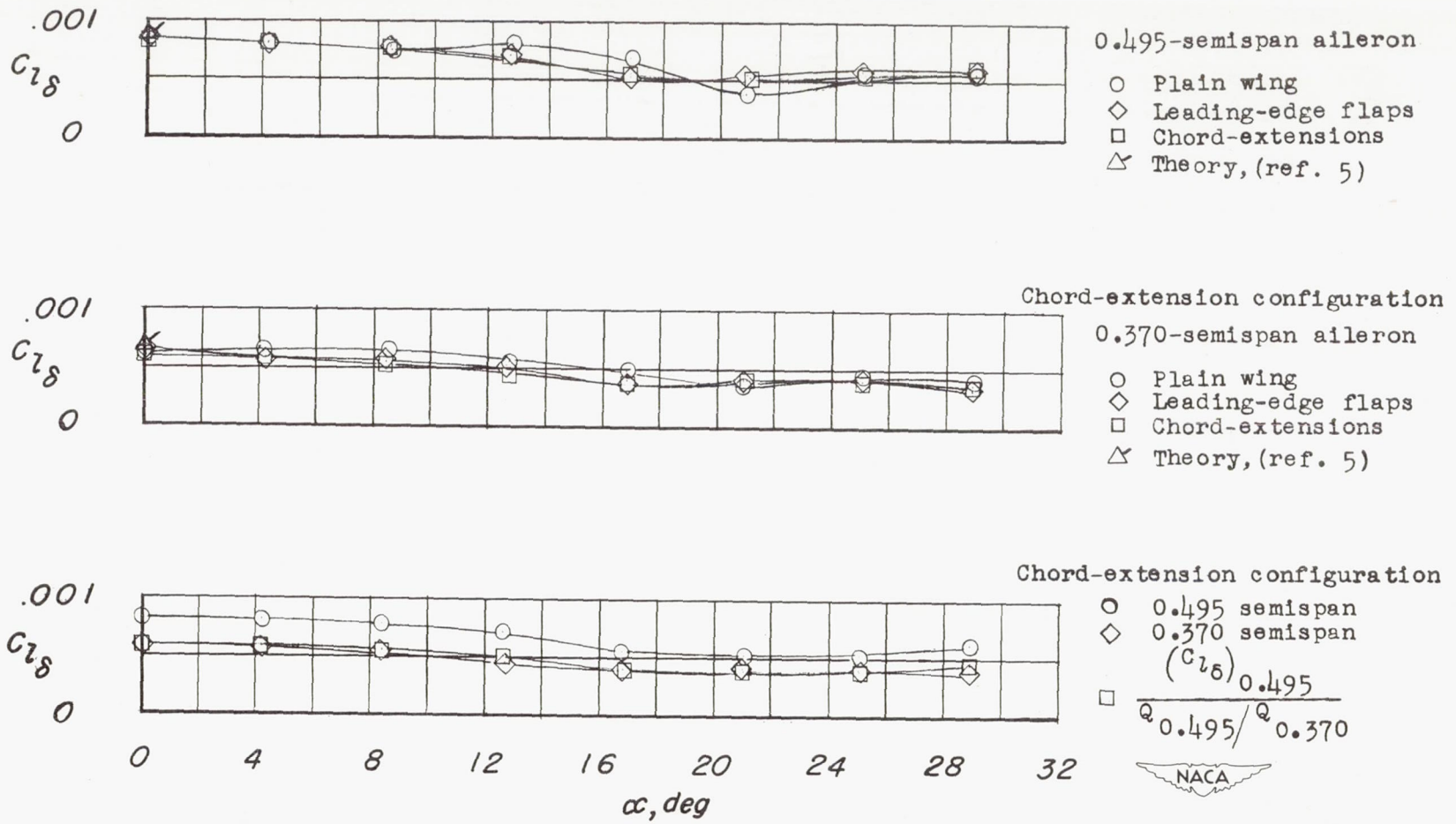


Figure 14.- Effects of chord-extensions and extensible leading-edge flaps on aileron effectiveness parameter C_{l_δ}. Symbols do not indicate test data.

NACA-Langley - 4-29-53 - 325